

UCSF

UC San Francisco Electronic Theses and Dissertations

Title

Regulation of Active Zone Assembly and Function by a Newly-Identified Serine-Arginine Protein Kinase

Permalink

<https://escholarship.org/uc/item/4223g8zr>

Author

Johnson, Ervin LeRoy

Publication Date

2009

Peer reviewed|Thesis/dissertation

Regulation of Active Zone Assembly and Function by a Newly-Identified Serine-

Arginine Protein Kinase

by

Ervin LeRoy Johnson III

DISSERTATION

Submitted in partial satisfaction of the requirements for the degree of

DOCTOR OF PHILOSOPHY

in

Neuroscience

in the

GRADUATE DIVISION

of the

UNIVERSITY OF CALIFORNIA, SAN FRANCISCO

Copyright (2009)

by

Ervin LeRoy Johnson III

ii

Acknowledgements

I would like to express my extreme gratitude to the many people that have supported me throughout my graduate career. My thesis advisor, Grae Davis, has been an excellent mentor and an impressive role model. I can only hope to have adopted some of his fearless approach to science and scientific inquiry during my time in his laboratory. I am also grateful to the many members of the Davis lab with whom I have had the great fortune to overlap with. Without exception, Davis lab members have been supportive and generous with their time. I would also like to sent special thanks to Gama Ruiz, for keeping the Davis lab running; to Rick Fetter for donating his expertise in conducting all of the electron microscopy experiments in this thesis; and to Cathy Massaro and Sharon Bergquist for sharing this journey with me and making sure I had fun every step of the way.

Early in graduate school I reached a crossroads at which I had to decide whether or not to continue in scientific research. With input and advice that I received from a group formal and informal advisors, I decided to stay in graduate school and I today am certain that this was the correct path for me. I will forever be grateful to Grae Davis, Louis Reichardt, Robert Edwards, Kevin Shannon, Steve Finkbeiner, Larry Tecott, Huidy Shu, and Audrey Foster-Barber for their council.

I could not have made it through graduate school were it not for friends and colleagues in my Medical Scientist Training Program and Neuroscience Program classes. I feel so fortunate to have had the opportunity to be around such a diverse group of kind, generous, intelligent people. Wherever our futures take us, I hope that we keep in touch.

Words cannot express the debt that I owe to my family. My parents provided many life lessons in my early years that have benefited me to this day. Since my early teens, my mother has almost single-handedly kept our family on course. In recent years it has been a pleasure to witness my little sister growing into a beautiful, successful woman. I have truly been blessed.

Regulation of Active Zone Assembly and Function by a Newly- Identified Serine-Arginine Protein Kinase

by

Ervin LeRoy Johnson III

Abstract

Despite a voluminous knowledge concerning the ultrastructural and molecular composition of active zones, very little is known about how these presynaptic specializations are assembled. Furthermore, with a few exceptions little is known about the roles that active zone molecules play in synaptic function. In this thesis, I describe the identification and characterization of *Drosophila* mutants for a newly-identified serine-arginine protein kinase, which has been termed serine-arginine protein kinase at 79D (SRPK79D).

In Chapter 2 I describe a series of experiments involving quantitative imaging, electron microscopy and electrophysiology. The results of these experiments indicate that

SRPK79D is a negative regulator of T-bar assembly and have lead to a new model of active zone assembly. Specifically, the data suggest that in *wild type* animals active zone constituents are transported from the cell soma to the synapse where they are locally assembled. During transport assembly of these components must be constitutively repressed through the action of SRPK79D to prevent ectopic T-bar formation.

In Chapter 3 I present the initial characterization of a synaptic function deficit at the neuromuscular junction of *srpk79D* mutants. In otherwise *wild type* animals, over-expression of the vesicular glutamate transporter (VGlut) leads to an increase in the amplitude of spontaneous fusion events (minis) and an inversely-proportional, compensatory decrease in the average number of vesicles that fuse in response to presynaptic stimulation. Thus, through this process, which we term reverse homeostatic compensation, the average postsynaptic response to presynaptic stimulation in VGlut over-expressing animals is identical to animals expressing normal levels of VGlut. In *srpk79D* mutants, VGlut over-expression causes an identical increase in the average mini amplitude. Reverse homeostatic compensation also ensues. However, compensation is excessive. Consequently, the average postsynaptic response to presynaptic stimulation is approximately one-half that of *wild type* animals or animals that over-express VGlut but are *wild type* for *srpk79D*.

To date, *srpk79D* is the first gene shown to be involved in reverse homeostatic compensation. Furthermore, *srpk79D* is the first gene known to be required to dampen homeostatic compensation. Finally, the data suggest that destabilization of the T-bar may be required for reverse homeostatic compensation, which would represent a novel mechanism in modulation of synaptic efficacy.

Table of Contents

Acknowledgements.....	iii
Abstract.....	v
Table of Contents.....	vi
List of Figures and Tables.....	ix
Chapter One: General Introduction.....	1
<i>Active Composition and Function.....</i>	<i>4</i>
<i>Active Zone Assembly.....</i>	<i>9</i>
Chapter Two: Negative-Regulation of Active Zone Assembly by a Newly-Identified Serine-Arginine Protein Kinase.....	12
<i>Summary.....</i>	<i>13</i>
<i>Results.....</i>	<i>14</i>
<i>Discussion.....</i>	<i>29</i>
<i>Figures.....</i>	<i>35</i>
<i>Supplementary Discussion Relevant to Figure 2-8.....</i>	<i>64</i>
Chapter Three: SRPK79D is Required for Proper Homeostatic Regulation of Synaptic Efficacy.....	65
<i>Summary.....</i>	<i>66</i>
<i>Introduction to Synaptic Homeostasis.....</i>	<i>67</i>
<i>Results.....</i>	<i>69</i>
<i>Discussion.....</i>	<i>70</i>
<i>Figures.....</i>	<i>73</i>
Chapter Four: General Conclusions.....	75
<i>Identifying the SRPK79D target.....</i>	<i>76</i>
<i>Relieving SRPK79D-dependent repression.....</i>	<i>78</i>
<i>Assembly of Cytosolic Proteins.....</i>	<i>79</i>

Experimental Procedures.....	85
References.....	91
Publishing Agreement.....	100

List of Figures and Tables

<i>Figure 2-1. Brp Accumulates in srpk79D mutant nerves.....</i>	35
<i>Figure 2-2. Synaptic Brp deficit in srpk79D mutants.....</i>	38
<i>Figure 2-3. SRPK79D functions in neurons to prevent Brp accumulation.....</i>	40
<i>Figure 2-4. Kinesin-/Dynein-based axonal transport is intact in srpk79D mutants... </i>	42
<i>Figure 2-5. Comparison of synaptic and axonal Brp assemblies in wild type and srpk79D mutant animals.....</i>	44
<i>Figure 2-6. T-Bar super-assemblies are found in srpk79D mutant axons.....</i>	46
<i>Figure 2-7. Brp accumulation in srpk79D mutants is not due to increased Brp expression.....</i>	48
<i>Figure 2-8. SRPK79D kinase activity is necessary and the SRPK79D N-terminus directs targeting.....</i>	50
<i>Figure 2-9. SRPK79D over-expression disrupts synaptic Brp and impairs synapse function.....</i>	52
<i>Supplemental Figure 2-1. Analysis of synaptic Brp levels in anterior and posterior segments from wild type and srpk79D mutants.....</i>	54
<i>Supplemental Figure 2-2. Analysis of an additional srpk79D mutant.....</i>	56
<i>Supplemental Figure 2-3. Direct observation of Brp transport.....</i>	58
<i>Supplemental Figure 2-4. Supplemental molecular analysis.....</i>	60
<i>Supplemental Figure 2-5. Over-expression of SRPK79D-RD* causes synaptic Brp disruption.....</i>	62
<i>Figure 3-1. Improper execution of synaptic homeostasis in srpk79D mutants.....</i>	73

Chapter One:

General Introduction

Neurotransmission is the process by which information, in the form of electrical signals, is passed from neuron to neuron or from neuron to muscle cell. This form of intercellular signaling takes place at distinct sites of close cell-cell apposition called synapses. Depending upon the mechanism of signal transmission, synapses are classified as electrical and/or chemical. At electrical synapses, gap junctions connect the cytosolic compartments of synaptic partners and current can be passed directly from one cell to the other. Thus, electrical synaptic transmission is mechanistically simple and is therefore particularly rapid [Connors & Long 2004].

Despite being fast however, electrical neurotransmission has its limitations. For example, electrical synapses can only be sign-conserving. That is, depolarization of the upstream or presynaptic, neuron can only lead to passage of depolarizing current across an electrical synapse; and likewise, presynaptic hyperpolarization causes passage of hyperpolarizing current. Additionally, signal strength tends to diminish across electrical synapses because gap junctions resist current flow [Connors & Long 2004].

At chemical synapses in contrast, deflections in the presynaptic membrane potential are uncoupled from the downstream or postsynaptic cell's response. Chemical synapses can therefore be sign-conserving or sign-reversing, and both signal augmentation and diminishment are possible. These features permit many more possibilities for interconnecting neurons, a fact that is exploited broadly in the nervous system [Cowan & Kandel 2001].

The diversity of connectivity options made possible by chemical neurotransmission comes at the cost of mechanistic simplicity however. Indeed, a series of complex processes are involved, which include 1) calcium ion influx through

presynaptic calcium channels, 2) calcium-triggered fusion of neurotransmitter-filled synaptic vesicles with the presynaptic membrane, 3) diffusion of neurotransmitter across an intercellular space called the synaptic cleft, 4) binding of neurotransmitter by postsynaptic receptors, and finally 5) transduction of neurotransmitter binding into a change in postsynaptic membrane conductance properties [Cowan & Kandel 2001]. Chemical neurotransmission is therefore comparatively slow and metabolically costly. However, thanks to a series of molecular and morphological specializations, the sacrifices in speed and efficiency are minimized, allowing chemical neurotransmission to be the prevalent mechanism of neurotransmission throughout most metazoan nervous systems.

A particularly important specialization is the presynaptic active zone (AZ). This term was coined in 1970 by Couteaux and Pecot-Decavassine during an ultrastructural study of partially-contracted frog muscles. The authors observed that synaptic vesicle fusion tended to occur at specific regions of the presynaptic membrane and termed them 'les zones actives' [Couteaux and Pecot-Decavassine 1970]. Each AZ was also found to be in perfect alignment with a post-synaptic specialization called the junctional fold, which is especially rich in neurotransmitter receptors [Anderson & Cohen 1974]. Thus, by promoting synaptic vesicle fusion to a presynaptic membrane domain that directly opposes a postsynaptic region where neurotransmitter receptors are enriched, AZs maximize the speed, efficacy and efficiency of chemical neurotransmission.

Couteaux and Pecot-Decavassine also noted that AZs were peculiar for the a thickened, electron-dense presynaptic membrane; a region of high electron density projecting from the membrane into the cytoplasm; and a particularly high density of

synaptic vesicles in the immediately surrounding presynaptic volume [Couteaux and Pecot-Decavassine 1970].

Ultrastructural investigation of AZs at other synapses and in other species in the decades since Couteaux and Pecot-Decavassine's seminal study has proven their initial description to be quite generalizable. That is, all AZs possess a region of electron-dense membrane from which extends a cytosolic domain of high electron density. Furthermore, advances in ultrastructural imaging techniques and molecular genetics have further refined the understanding of AZ structure and function.

In this section I outline the current understanding of AZ composition at the ultrastructural and molecular levels. Where data are available I also discuss the roles of active zone specific molecules in synaptic transmission. I go on to summarize what is known about AZ formation, including the transport of AZ components to nascent and mature synapses and the assembly and integration of these components into a functional AZ.

Active Zone Composition and Function

The basic ultrastructural description of AZs has largely come from thin-section transmission electron microscopic imaging. However, a variety of other ultrastructural imaging techniques have been employed to refine this simple description. The electron-dense cytosolic domain in particular has received a great deal of attention. Additionally, through a combination of biochemistry, immunoelectron microscopy and molecular genetics a molecular characterization of each of these AZ components has begun to emerge.

Active Zone Membrane

The electron-dense nature of the AZ membrane is believed to reflect an especially high concentration of transmembrane and membrane-associated proteins. Among these proteins are voltage-sensitive calcium channels and the target-SNARE proteins syntaxin and SNAP-25. Together with the vesicle-SNAREs synaptobrevin, syntaxin and SNAP-25 form a high energy complex that is believed drive fusion of the active zone and vesicle membranes [Rizo & Rosenmund 2008]. Thus, the vesicle-fusion trigger (intracellular calcium) and the fusion machinery (SNARE-complex) are co-localized at the AZ-membrane, which at least partly explains its vesicle fusion competence [Rizo & Rosenmund 2008].

Various classes of cell adhesion molecules (CAMs) are also found at the AZ membrane. Through trans-synaptic interactions with postsynaptic CAMs, these molecules maintain close apposition synaptic partner membranes. Moreover, these molecules are likely candidates for keeping presynaptic release sites and postsynaptic receptor-rich specializations in register [Akins & Biederer 2006, Budnik 2007]. Interestingly, some classes of AZ CAMs have important roles in signaling during neurodevelopment and synapse differentiation. Thus, it is possible that in addition to maintaining structural integrity, some CAMs play a role in trans-synaptic signaling in mature synapses [Clandinin & Zipursky 2002, Akins & Biederer 2006].

Cytomatrix of the AZ

Another ultrastructural feature common to all AZs is an electron-dense region that fills the cytosolic volume immediately adjacent to the AZ membrane. Closer examination of this region at various synapses has shown that the high electron density actually

reflects an organized network of protein fibrils. In an effort to provide a name that better reflects its organized nature, this electron-dense region has recently been termed the cytomatrix of the AZ (CAZ).

In a particularly noteworthy study of the CAZ Harlow and colleagues used electron microscopy tomography to achieve a high resolution picture of the active zone material within 15nm of the membrane at the frog neuromuscular junction (NMJ) [Harlow et al 2001]. The authors determined that this AZ region contains a highly organized network composed of at least three classes of cytoplasmic filaments, which they termed “beams”, “ribs” and “pegs”. According to their model, a series of beams run parallel to the plasma membrane and specify the longitudinal axis of the AZ. Ribs project from beams, roughly perpendicular to the longitudinal AZ axis and interact with so called “docked” synaptic vesicles at their distal ends. Pegs project from ribs into the plasma membrane where they contact voltage-gated calcium channels [Harlow et al. 2001].

Molecularly, the CAZ has been shown to contain different classes of cytoskeletal proteins, including Actin and Spectrin as well as scaffolding proteins such as CASK and PSD-95 [Zhai & Bellen 2004]. Of particular interest, several families of AZ-specific molecules have also been shown to localize to the CAZ [Zhai & Bellen 2004, Schoch & Gundelfinger 2006]. These include phylogenetically old genes such as *C. elegans* unc-13, unc-10, and ELKS; which have orthologues in flies and vertebrates, as well as proteins such as Bassoon & Piccolo, which have only been identified in vertebrate species and presumably represent newer evolutionary innovations.

The roles of several of the AZ-specific proteins have also been evaluated. For example, the fly and mouse homologues of unc-13, (Dunc-13 and Munc-13, respectively)

appear to be dispensable for AZ structure, but are absolutely required for vesicle fusion at excitatory synapses [Aravamudan et al. 1999, Richmond et al. 1999, Varoqueaux et al. 2002]. Similarly, AZ ultrastructure is not affected in mutants for the mammalian orthologue of *unc-10*, termed RIM. However, certain forms of synaptic plasticity are abolished [Kaeser & Sudhof 2005]. In contrast, AZ architecture is profoundly disrupted in Bassoon mutants, but vesicle fusion per se is normal (however see below) [Dick et al. 2003, Khimich et al. 2005].

Active Zone Cytosolic Projections

At many synapses the CAZ is further specialized, forming one or more electron dense structures that are anchored to the AZ membrane and project into the cytosol [Zhai & Bellen 2004]. While these projections vary greatly in shape and size they appear to be especially prominent at AZs of high-releasing terminals such as those of motoneurons and photoreceptors.

The prototypical cytosolic projection, found at vertebrate photoreceptor and hair cell terminals, is the synaptic ribbon. Long and thin in cross-section, these structures project up to several hundred nanometers into the presynaptic cytoplasm. Interestingly, hundreds of synaptic vesicle profiles are found to be directly associated with ribbons.

Recently, tom Dieck and colleagues combined immunocytochemical and immunoelectron microscopy techniques to provide an impressive molecular description of synaptic ribbons [tom Dieck et al. 2005]. The authors segregate the ribbon into two molecularly distinct domains: the arciform complex, which abuts the presynaptic membrane and the ribbon proper. The arciform complex is rich in the mammalian ELKS homologue ERC2/CAST1, Munc13-1, and RIM2. The suspected scaffolding protein

Bassoon on the other hand localizes to a domain that defines the molecular interface between the arciform complex and the ribbon. The major constituent of the ribbon proper was found to be the protein RIBEYE, a splice variant of the RNA-binding protein CtBP2 that interacts with Bassoon. Also found in the ribbon are the AZ-specific proteins Piccolo and RIM1 as well as the kinesin KIF3A. Interestingly, the RIBEYE/CtBP2 homologue CtBP1, which has not thus far been shown to interact with any other AZ protein, was also found in the ribbon [Schmitz et al. 2000, tom Dieck et al. 2005].

Electrophysiological analysis of mouse mutants lacking a central domain of Bassoon has provided direct insight into ribbon function. In these mutants, ribbons progressively detach from the presynaptic membrane. Interestingly, while sustained vesicle release is preserved at these synapses, the capacity for synchronous vesicle release diminishes over a time course that mirrors ribbon detachment. Thus, the ribbon is not absolutely required for vesicle release, but it facilitates the rapid release of many synaptic vesicles [Khimich et al. 2005].

Another well characterized AZ cytosolic projection is the T-bar found at *Drosophila* motoneuron and tetrad photoreceptor synapses [Zhai & Bellen 2004]. As suggested by the term used to describe it, T-bar profiles approximate the letter “T” in cross-section. Similar to ribbons, T-bars are often found in close proximity to and often in direct contact with synaptic vesicles. However in contrast to the ribbon, little is known about the molecular composition of T-bars. In fact, with the exception of the ELKS/ERC homologue Bruchpilot (Brp), data to support the presence of any other protein in the T-bar are lacking.

Consistent with the conclusion that Brp is a major T-bar constituent, T-bars are absent in Brp null larvae. Furthermore, electrophysiological analysis of *brp* mutant NMJs revealed diminished vesicle release in response to stimulation. This finding was coincident with decreases in both the number of peri-AZ synaptic vesicles and the clustering of presynaptic calcium channels.

Active Zone Assembly

In contrast to the great deal of knowledge concerning AZ composition and function that has emerged since the early 1970s, relatively little is known about AZ formation. Mechanisms important for the delivery of AZ constituents to nascent synapses have been identified. And interestingly, there are data to support a model in which AZ components are pre-packaged and transported together from the cell soma to the synapse. This model further allows for the possibility that AZ components are transported as pre-assembled, functional or partially functional units.

Axonal Transport

Current data indicate that like other proteins destined for the synapse, AZ proteins are translated in the cell soma and transported to the synaptic terminal via microtubule-based axonal transport [Hurd & Saxton 1996, Pack-Chung et al. 2008]. Consistent with this model, in *Drosophila*, loss-of-function mutations in *kinesin heavy chain*, *kinesin light chain* and *dynein heavy chain* lead to the formation of large “axonal swellings” that contain Brp [Hurd et al. 1996, Martin et al. 1999]. Additionally, in mutants for the gene *immaculate connections*, which encodes a Kinesin 3 family member, transport of

synaptic proteins, including Brp is completely abolished by late embryonic stages [Pack-Chung et al. 2008].

Active Zone Precursor Vesicles

In cultured hippocampal neurons, transport vesicles containing active zone components including the calcium channel α 1a subunit have been described [Ahmari et al. 2000]. Similarly, Zhai and colleagues described dense core vesicles associated with Bassoon and Piccolo [Zhai et al. 2001]. These studies have led to an interesting AZ assembly model whereby AZ molecules are pre-packaged in association with vesicles in the cell soma and transported to nascent synapses. Upon reaching the synaptic terminal, these active zone transport vesicles (AZTVs) fuse with the presynaptic membrane to thereby depositing their cargo [Ahmari et al. 2000, Zhai et al. 2001, Shapira et al. 2003, Dresbach et al. 2006].

This is an intriguing model. However, several questions remain. First, upon reaching the nascent synapse what mechanisms promote the assembly of AZ components into a functional AZ? Conversely, what prevents ectopic assembly of AZ constituents into macromolecular AZ structures during transport? Furthermore, how is the correct location of AZ assembly specified?

In the following chapter of this thesis, I describe the characterization of a newly identified *Drosophila* serine-arginine protein kinase termed “*serine-arginine protein kinase at 79D*” (srpk79D). SRPK79D is expressed in neurons and co-localizes with Brp both in axons and at the synapse. Loss-of-function mutations in *srpk79D* lead to large Brp accumulations in larval axons. Ultrastructural examination of *srpk79D* mutant larval nerves reveals ectopic T-bar-like structures. Furthermore, over-expression of SRPK79D

disrupts synaptic Brp assembly and impairs synaptic function. Together these data identify kinase-dependent suppression as a novel mechanism in the regulation of AZ assembly and suggest that site-specific relief of suppression specifies the location of AZs.

In Chapter 3, I describe the initial characterization of a synaptic function deficit in *srpk79D* mutants. Interestingly, this deficit is revealed only in a context in which a *wild type* synapse would typically respond by reducing stimulus-evoked vesicle fusion. To our knowledge, SRPK79D is the only molecule shown to be involved in this process. Finally, in Chapter 4 I discuss this newly identified SRPK79D-dependent mechanism for regulating AZ assembly in the context of other examples of regulated cytosolic protein assembly.

Chapter Two:

Negative Regulation of Active Zone Assembly by a
Newly-Identified SR-Protein Kinase

Summary

Presynaptic, electron-dense, cytoplasmic protrusions such as the T-bar (*Drosophila*) or ribbon (vertebrates) are believed to facilitate vesicle movement to the active zone (AZ) of synapses throughout the nervous system. The molecular composition of these structures including the T-bar and Ribbon are largely unknown, as are the mechanisms that specify their synapse-specific assembly and distribution.

In a large scale, forward genetic screen we have identified a mutation termed *air traffic controller* (*atc*) that causes T-bar-like protein aggregates to form abnormally in motoneuron axons. This mutation disrupts a gene that encodes for a serine-arginine protein kinase (SRPK79D). This mutant phenotype is specific to SRPK79D and is not secondary to impaired kinesin-dependent axonal transport. The *srpk79D* gene is neuronally expressed and transgenic rescue experiments are consistent with SRPK79D kinase activity being necessary in neurons. The SRPK79D protein co-localizes with the T-bar associated protein Bruchpilot (Brp) in both the axon and synapse. We propose that SRPK79D is a novel T-bar associated protein kinase that represses T-bar assembly in peripheral axons, and that SRPK79D-dependent repression must be relieved to facilitate site-specific AZ assembly. Consistent with this model, over-expression of SRPK79D disrupts active-zone specific Brp organization and significantly impairs presynaptic neurotransmitter release.

These data identify a novel AZ-associated protein kinase and reveal a new mechanism of negative regulation involved in active zone assembly. This mechanism could contribute to the speed and specificity with which active zones are assembled throughout the nervous system.

Results

***srpk79D* loss of function causes Bruchpilot accumulation in larval nerves**

In an ongoing screen to identify genes involved in the formation and stabilization of the *Drosophila* NMJ we identified a P-element insertion (P10036) in which the peripheral nerves contain numerous large accumulations of the AZ associated protein Bruchpilot (Brp, Fig. 2-1E – 2-1G). These large, aberrant Brp accumulations ranged from roughly spherical to grossly elongated in appearance (Fig. 2-1E – 2-1G). In *wild type* animals, by contrast, axons within the peripheral nerves showed virtually no anti-Brp staining and the Brp puncta that did appear in these axons were small and spherical in appearance (Fig. 2-1B – 2-1D).

This phenotype is very unusual based upon the results of our ongoing genetic screen. In this forward genetic screen we have analyzed over 2000 independent transposon insertion lines, including PiggyBac lines on chromosomes 2 and 3 from the Exelixis collection and an independent collection of P{GAL4} lines [Thibault et al. 2004]. In each mutant background we have stained 3-5 larvae with anti-Brp and anti-Discs Large (Dlg) antibodies and examined both the peripheral nerves and the neuromuscular synapse for defects. P10036 is the only mutation identified to date that causes the observed accumulation of anti-Brp staining in peripheral axons. The P10036 transposon resides within an intron of the previously uncharacterized gene *CG11489*, which resides at chromosomal position 79D and is predicted to encode a member of the serine-arginine protein kinase (SRPK) family (see below, Fig. 2-1A, 2-8A, 2-8B). Due to the dramatic effect on Bruchpilot (German for crash pilot) protein accumulation in

peripheral axons, we named this mutant *air traffic controller (atc)*, and we refer to P10036 as *srpk79D^{atc}* throughout this manuscript.

We next developed quantitative measures of the axonal Brp accumulations to further characterize and analyze the *srpk79D^{atc}* mutant phenotype (see methods). In all cases, genetic controls were dissected, processed, stained and imaged identically and in parallel with *srpk79D^{atc}* mutants. We found a statistically significant increase in total nerve Brp fluorescence in *srpk79D^{atc}* mutants compared to *wild type* and heterozygous controls ($p < 0.001$, student's t-test; Fig. 2-1K). We also found a highly significant increase in the average puncta fluorescence intensity compared to *wild type* and heterozygous controls. Indeed, the entire distribution of puncta intensities was shifted toward larger values ($p < 0.001$, Mann-Whitney U Test; Fig. 2-1L). Finally, we estimate that the frequency of these aberrant accumulations corresponds to 0.03 accumulations per micron of individual motor axon length. From these data we conclude that Brp-positive puncta in *srpk79D^{atc}* mutant axons represent larger protein aggregates than observed in *wild type* axons.

Next we assayed synaptic Brp staining intensity and neuromuscular junction (NMJ) morphology in the *srpk79D^{atc}* mutant. We found that synaptic Brp staining intensity is significantly decreased compared to *wild type* animals, assayed as both total Brp fluorescence ($p < 0.001$, student's t-test; Fig. 2A-2E) and as the distribution of individual puncta intensities ($p < 0.001$, Mann-Whitney U Test; Fig. 2-2A – 2-2D, 2-2F). This effect occurs at NMJ throughout the animal and there is no evidence for a strong anterior-posterior gradient of this phenotype (Fig. 2- S1A). Our data suggest that the accumulation of Brp aggregates in the axon of the *srpk79D^{atc}* mutant depletes Brp protein

from the presynaptic nerve terminal. Consistent with this conclusion, we found that total Brp protein levels, assayed by Western blot, are unaltered in the *srpk79D^{atc}* mutant background despite the dramatic increase in nerve Brp (see below).

We also determined whether the decrease in total Brp fluorescence causes a decrease in total Brp puncta number, which would be indicative of a change in AZ number. We found, however, that Brp puncta density within *srpk79D^{atc}* mutant NMJs is identical to *wild type* and that total bouton numbers were wild type in the *srpk79D^{atc}* mutant background (Fig. 2-2G, 2-2H). Moreover, anti-Dlg, anti-Synaptotagmin 1 (Sy1) and anti-Cysteine String Protein (CSP) staining at *srpk79D^{atc}* mutant synapses are not different compared to *wild type* (data not shown). Thus, synapse growth, morphology and AZ number appear normal in the *srpk79D^{atc}* mutant.

Consistent with this observation we found no change in neurotransmitter release in the *srpk79D^{atc}* mutant background. We assayed neurotransmission by recording from the third instar NMJ of homozygous *srpk79D^{atc}* mutants, as well as homozygous *srpk79D^{atc}* mutants lacking one copy of the *brp* gene (*brp^{69/+};srpk79D^{atc}*) [Kittel et al. 2006]. In all cases, evoked excitatory junctional potential (EJP) amplitude and spontaneous miniature EJP (mEJP) amplitudes were *wild type*, as was the ability of the NMJ to sustain high frequency (10Hz) stimulation in high extracellular calcium saline (2mM) (data not shown; see below, however, for additional electrophysiological analyses). Thus, the *srpk79D^{atc}* mutants possess inappropriate axonal accumulations of Brp protein, resulting in a depletion of this synaptic protein from the presynaptic AZ. However, the degree of depletion of Brp from the NMJ does not cause a defect in synaptic function over the time course of 4 days of larval development.

SRPK79D is expressed in the embryonic CNS and is required in larval motoneurons

We have used our quantitative assays to confirm that the phenotype of axonal Brp accumulation is caused by disruption of the *srpk79D* gene and to determine the nature of this genetic disruption. First, we demonstrated that the axonal Brp accumulation and synaptic Brp deficit phenotypes in the homozygous *srpk79D^{atc}* mutant are statistically identical to those observed when the *srpk79D^{atc}* mutation is placed *in trans* to a deficiency chromosome that uncovers the *srpk79D* gene locus, *Df(3L)Exel6138* (Fig. 2-1E – 2-1L, 2-2E, 2-2F). Furthermore, the axonal and synaptic Brp phenotypes in homozygous *srpk79D^{atc}* mutants are statistically identical to those observed in mutants homozygous for a recently identified molecular null allele of the *srpk79D* gene (*srpk79D^{l^{N100}}*, Fig. 2-S2A – 2-S2H) [Nieratschker et al. *in review*]. These data are consistent with the conclusion that the *srpk79D^{atc}* transposon insertion is a strong loss-of-function or null mutation in the *srpk79D* gene. Interestingly, we found that the heterozygous *srpk79D^{atc}/+* mutant axons also have slight but statistically significant increase in Brp fluorescence compared to *wild type*. These data indicate that *srpk79D* is partially haploinsufficient for the regulation of axonal Brp accumulation.

Next, we determined the expression pattern of the *srpk79D* gene. *In situ* hybridizations performed on *wild type Drosophila* embryos targeting an exon common to all known *srpk79D* transcripts (Fig. 2-8A, also see methods) detected high levels of *srpk79D* mRNA in the embryonic ventral nerve cord with lower expression present outside of the nervous system (Fig 2-3A, 2-3B). This expression pattern is consistent with a function of *srpk79D* gene products in neurons, but does not rule out a possible function in other tissues including peripheral glia.

To confirm that loss of *srpk79D* is responsible for the phenotype of axonal Brp accumulation, and to determine where *srpk79D* is required for normal Brp targeting, we employed a *srpk79D* RNAi transgene (*UAS-srpk79D^{RNAi}*, Vienna Drosophila RNAi Collection). We found that expression of *UAS-srpk79D^{RNAi}* in neurons phenocopies the *srpk79D^{atc}* mutation (Fig. 2-3C – 2-3F), while expression of *UAS-srpk79D^{RNAi}* in glia (also present in peripheral nerve) does not cause formation of axonal Brp aggregates. These data indicate that *srpk79D* function is required in neurons, consistent with enriched expression in the central nervous system.

We also performed a genetic rescue experiment by expressing a Venus-tagged, full-length *srpk79D* transgene (*UAS-v-srpk79D-rd**) in neurons in the homozygous *srpk79D^{atc}* mutant background. In this experiment, neuronal expression of *UAS-v-srpk79D-rd** significantly rescued the *srpk79D^{atc}* mutant phenotype toward *wild type* levels (Fig. 2-3G – 2-3J). The presence of axonal Brp accumulations was reduced (Fig. 2-3G, 2-3H) and there was a correlated increase in synaptic Brp fluorescence in the rescue animals compared to the mutation (data not shown). Taken together, our data are consistent with the conclusion that loss of *srpk79D*, in neurons, is responsible for the abnormal accumulation of Brp in peripheral nerves.

Finally, we noted that the *srpk79D* gene resides just downstream of the gene encoding CSP. In mammals, CSP was recently shown to suppress axonal protein aggregation [Fernandez-Chacon et al. 2004]. Therefore, we pursued additional experiments to determine whether disruption of the *Csp* gene might participate in the phenotype of Brp axonal accumulation. In these experiments we took advantage of a strong hypomorphic *Csp* allele in which the 5' region of the *Csp* gene is deleted and the

srpk79D locus is intact (*Csp^{XI}*, Fig. 1A) [Eberle et al. 1998]. When *srpk79D^{atc}* was placed *in trans* to the *Csp^{XI}* mutation, we found a modest increase in Brp fluorescence and Brp puncta intensity compared to *wild type*, but not compared to the *srpk79D^{atc/+}* heterozygous mutant (Fig. 2-1K, 2-1L). Based upon these data we conclude that *Csp* is not directly involved in the phenotype of increased axonal Brp puncta staining observed in the *srpk79D* mutant.

Evidence that axon transport is intact in *srpk79D* mutants

To date, the formation of axonal protein aggregates has been documented in *Drosophila* larvae that are mutant for genes that disrupt both retrograde and anterograde axonal transport [Hurd & Saxton 1996, Martin et al. 1999, Miller et al. 2005, Pilling et al. 2006]. For example, mutations in *kinesin heavy chain* and disruption of the Dynein/Dynactin protein complex cause large axonal aggregates composed of diverse synaptic proteins and organelles including, but not limited to, Syt, CSP, Dap160/Intersectin (Dap160) mitochondria and Brp [Hurd & Saxton 1996, Martin et al. 1999, Pilling et al. 2006]. Thus, we considered the possibility that the *srpk79D^{atc}* mutation disrupts axonal transport by asking whether additional synaptic proteins accumulate with Brp in the *srpk79D^{atc}* mutant axons. We found, however, that the distribution of Syt, CSP, mitochondria, Dap160 and Liprin-alpha were all unchanged relative to *wild type* in the *srpk79D^{atc}* mutants (Fig. 2-4A – 2-4L). We also find over-expressed EGFP-CaV2.1 is wild type in the *srpk79D^{atc}* mutants (data not shown) [Kawasaki et al. 2004]. Thus, the *srpk79D^{atc}* mutation seems to specifically disrupt the transport or aggregation of the Brp protein in peripheral axons without affecting the transport of synaptic vesicles or other AZ constituent proteins.

We next explored the possibility that SRPK79D participates in the specific transport of Brp protein. In recent years, proteins have been identified that are specifically required for the anterograde transport of synaptic proteins or other cellular organelles such as mitochondria [Martin et al. 1999, Guo et al. 2005, Pack-Chung et al. 2007]. SRPK79D is not strictly required for axonal transport of Brp because Brp protein is present at the NMJ in the *srpk79D^{atc}* mutant. However, it is possible that SRPK79D facilitates the anterograde transport of Brp/T-bars. Therefore, we pursued genetic interactions between *srpk79D* and either *kinesin heavy chain (Khc)* or *kinesin 3 (immaculate connections; imac)* [Hurd & Saxton 1996, Pack-Chung et al. 2007]. Larval nerves that are heterozygous for the amorphic *Khc⁸* allele contain rare “axonal swellings” that contain Syt, CSP, Brp, Dap160 and KHC [Hurd & Saxton 1996] (E.L.J. and G.W.D. unpublished observations). Importantly, these swellings can be clearly distinguished from the axonal Brp accumulations observed in *srpk79D* mutants because Brp accumulations in *srpk79D^{atc}* do not contain any other known synaptic protein. Therefore, we are able to assess whether the presence of a heterozygous *Khc* or *imac* mutation would enhance the *srpk79D^{atc}* mutant phenotype by increasing the abundance of Brp-specific protein aggregates in animals co-labeled with anti-Brp and an additional synaptic protein. If SRPK79D facilitates axonal transport of Brp, then reducing KHC or Imac protein levels should enhance the *srpk79D* mutant phenotype (Brp-specific protein aggregates). However, we found that placing a heterozygous *Khc⁸ /+* or *imac¹⁷⁰ /+* mutation in an *srpk79D^{atc}* homozygous mutant background (*Khc⁸ /+; srpk79D^{atc}* or *imac¹⁷⁰ /+; srpk79D^{atc}*) affected neither the frequency nor the severity of the Brp-specific axon aggregates characteristic of the *srpk79D^{atc}* mutant, nor was there any difference in the axonal

swellings characteristic of the *Khc* mutant (multi-protein aggregates) (Fig. 2-4M, 2-4N). We then repeated this experiment using numerous additional mutations in the *Khc* gene as well as other genes implicated in axonal transport including: 1) the antimorphic *Khc*¹⁶ allele [Hurd & Saxton 1996], 2) *Df(3L)34ex5*, which deletes the *kinesin light chain* locus [Gindhart et al. 1998], and 3) the amorphic *dynein heavy chain at 64C* allele *Dhc64C*⁴⁻¹⁹ [Gepner et al. 1996]. We also analyzed double mutants for *srpk79D* and *liprin-alpha* (*lip-α*), an AZ protein shown to play a role in axon transport [Kaufman et al. 2002] (*lip-α*^{R60}/*lip-α*^{F3ex5}; *srpk79D*^{atc}). None of these perturbations had any effect on Brp-specific protein accumulations in axons (data not shown). Finally, through direct observation, we find that small Brp puncta continue to be transported along axons in the *srpk79D*^{atc} mutant larval nerves, whereas large aggregates appear to be stalled (Fig. 2-S3). Taken together, our genetic and live imaging support the conclusion that Brp accumulations observed in *srpk79D* mutants are not due to a general defect in axonal transport.

Finally, we asked whether T-bars might be pre-assembled structures that are trafficked to the NMJ and inserted at the AZ. In some mutant backgrounds, T-bars have been observed to dislodge from the synapse and reside in the cytoplasm [McCabe et al. 2003]. However, we have never observed the appearance of T-bar-like structures in *wild type* *Drosophila* axons at the ultrastructural level (R.D.F. and G.W.D., unpublished observation). This suggests that T-bars are normally assembled at the presynaptic AZ. To examine this question further we analyzed the size and intensity of anti-Brp puncta in *wild type* axons and synapses. At the light level, the vast majority of Brp puncta in *wild type* axons are smaller and less intense than the puncta observed within the *wild type* presynaptic nerve terminal, suggesting that synaptic T-bars are assembled at the synapse

from constituent proteins, including Brp, that are transported down the axon to the synapse (Fig. 2-5). By contrast, Brp puncta observed in *srpk79D* mutants stained more intensely and were much larger than Brp puncta found in *wild type* axons. These Brp puncta were also often larger than the T-bar associated Brp puncta observed at *wild type* NMJ (Fig. 2-5). Thus, the large Brp accumulations found in *srpk79D* mutant axons could represent super-assemblies of T-bar related proteins, including Brp. To address this possibility, we examined *srpk79D* mutant axons ultrastructurally.

Evidence for premature T-bar assembly in *srpk79D* mutant axons

Mutations that cause focal accumulation of synaptic proteins in *Drosophila* nerves have been described previously and ultrastructural analyses have been carried out for three of these mutants. In *Khc* and *Dhc64C* mutants, axons become dramatically enlarged and are filled with an array of membrane-bound organelles including multivesicular bodies, pre-lysosomal vacuoles, and mitochondria [Hurd & Saxton 1996, Martin et al. 1999]. In contrast, *lip- α* mutant axons have normal diameters and contain organelle accumulations composed predominantly of clear-core vesicles [Miller et al. 2005].

In the *srpk79D* mutant, we found that axon diameters were not significantly different from *wild type* (Fig. 2-6A, 2-6B). Remarkably, and in contrast to all three of the mutants described above, we found that *srpk79D* mutant motor axons contained highly organized, electron-dense structures that were not surrounded by a vesicular or intracellular membrane compartment (Fig. 2-6A – 2-6C). Often, these electron-dense structures appeared strikingly similar to T-bars that had been joined at their “bases” into a large T-bar aggregate (Fig. 2-6C, 2-6D). We have never observed a similar structure in

wild type axons. The dimensions of these electron-dense structures, the prevalence of these structures in our EM sections and the similarity of their shape to T-bars present at the AZ strongly suggest that these structures represent the large Brp aggregates (super-assemblies) that we observe at the light level in the *srpk79D* mutant background. Finally, similar to T-bars found at AZs, these electron-dense structures were surrounded by a filamentous matrix (Fig 2-6A – 2-6D). Although vesicles were also observed in these areas, we believe that they are molecularly distinct from synaptic vesicles because synaptic vesicle markers do not co-localize with Brp in the *srpk79D* mutant axons (Fig 2-4A – 2-4L). In contrast, synaptic ultrastructure in *srpk79D* mutants is identical to *wild type* (data not shown). Thus, loss of *srpk79D* leads to the formation of T-bar-like super-assemblies in axons. Since we have never observed T-bar-like structures in *wild type* axons, we propose that SRPK79D is required as part of a mechanism that normally suppresses premature T-bar assembly in the axon.

SRPK79D co-localizes with Brp in the axon and at the active zone

To gain insight into the subcellular distribution of SRPK79D we generated Venus-tagged *srpk79D* transgenes under UAS control (UAS-*v-srpk79D*) and expressed these transgenes in Drosophila neurons. We found that neuronally expressed Venus-SRPK79D-RD*, which rescues axonal Brp accumulations (Fig. 2-3G – 2-3J), precisely co-localizes with Brp in both the nerve and at each presynaptic AZ (Fig. 2-8C – 2-8J). To our knowledge, the voltage-gated calcium channel Cacophony is the only other protein that has been demonstrated to co-localize with Brp at the presynaptic AZ [Kawasaki et al. 2004]. Furthermore, Venus-SRPK79D-RD* is the first protein that has been shown to co-localize with Brp in a *wild type* axon. These data suggest that SRPK79D closely

associates with Brp during axonal transport of the Brp protein to the presynaptic nerve terminal. It is possible that the distribution of the tagged-SRPK79D protein does not reflect the *wild type* SRPK79D protein distribution. However, the observation that Venus-SRPK79D-RD* shows a very restricted distribution, co-localizing with Brp in at least two cellular compartments, argues that this protein reflects, at least in part, the normal protein distribution.

Given that SRPK79D co-localizes with Brp, we considered two hypotheses for SRPK79D function. First, we considered the hypothesis that SRPK79D somehow influences total Brp protein levels in the cell, perhaps by influencing Brp stability or turnover. However, when we assayed total Brp protein levels by Western blot we found no change in the *srpk79D* mutant compared to *wild type* and no evidence of altered protein degradation (Fig. 2-S4B, 2-S4C). Although Western blots fail to measure Brp protein levels exclusively in motoneurons, this is consistent with our prior observation that axon Brp fluorescence increases while synaptic Brp decreases in the SRPK79D mutant, leaving total Brp protein levels constant in the cell. To further examine this possibility, we over-expressed a GFP-tagged *brp* transgene in otherwise *wild type* motoneurons using the GAL4-UAS expression system [Wagh et al. 2006]. Although this resulted in the accumulation of Brp protein within axons, GFP-Brp overexpression did not precisely phenocopy the *srpk79D* mutant. GFP-Brp expression simultaneously increased synaptic and axonal fluorescence, whereas *srpk79D* mutation causes increased axonal Brp and a correlated decrease in synaptic Brp (Figs. 2-1, 2-2, 2-7A – 2-7I). Thus, while Brp overexpression is sufficient to cause axonal aggregates, it seems unlikely that this is the cause of the defect in the *srpk79D* mutant. Consistent with this conclusion, co-

overexpression of BRP and SRPK79D-RD* does not reduce the severity of the axonal accumulations caused by BRP overexpression alone. To further address this issue, we asked whether Brp aggregates form in homozygous *srpk79D^{atc}* mutants in which we decrease total Brp levels by removing one copy of the *brp* gene (*brp^{69/+};srpk79D^{atc}*) [Kittel et al. 2006]. We found that large axonal Brp aggregates persisted even when one copy of the *brp* gene is removed in the background of the *srpk79D^{atc}* homozygous mutant (Fig. 2-7D, 2-7H, 2-7I).

Taken together, these experiments indicate that an ATC-dependent elevation in Brp protein is not the direct cause of premature T-bar-like assembly formation in the axon. We therefore favor an alternative model based upon the observation that SRPK79D co-localizes with Brp and speculate that SRPK79D could sequester or inhibit the function of axonal T-bar proteins and thereby prevent the formation of axonal T-bar-like super-assemblies.

SRPK79D kinase activity is necessary to prevent Brp accumulation.

As mentioned above, sequence analysis of the predicted *srpk79D* gene products reveals similarity to a group of serine-threonine kinases called SRPKs (Fig. 2-8B). Members of this protein kinase family share a characteristic split serine-threonine kinase domain [Nolen et al. 2001]. We therefore performed experiments to determine whether the kinase domain is required for SRPK79D activity. As shown earlier, transgenically expressed full-length SRPK79D (SRPK79D-RD*) co-localizes with Brp and rescues the *srpk79D* mutant phenotype. In contrast, expression of an SRPK79D isoform with a truncated kinase domain (SRPK79D-RD) co-localized with Brp, but failed to rescue the *srpk79D* mutant phenotype (Fig. 2-8B, 2-8K). These data indicate that the SRPK79D

kinase domain is involved in preventing axonal super-assemblies of Brp but that it is not important for co-localization with Brp. To further test the importance of SRPK79D kinase activity we generated a kinase dead *srpk79D* transgene by introducing a missense mutation into SRPK79D-RD* that is predicted to disrupt the ATP binding pocket of the kinase domain and thereby inhibit kinase activity (SRPK79D-RD*KD, Fig 2-8B). A similar strategy has been used previously to eliminate kinase activity in other SRPKs ranging from yeast to human [Colwill et al. 1996, Koizumi et al. 1999, Yeakley et al. 1999]. Like SRPK79D-RD*, SRPK79D-RD*KD co-localized with Brp. However, even when expressed at higher levels than SRPK79D-RD*, SRPK79D-RD*KD failed to rescue the *srpk79D* mutant phenotype (Fig. 2-8K and data not shown).

We next asked which domains might be required for SRPK79D protein trafficking and/or localization. We have found that an SRPK79D transgene that possesses an alternative SRPK79D N-terminal region but is otherwise identical to SRPK79D-RD* (SRPK79D-RB) failed to be efficiently trafficked out of the neuronal soma, was not found to co-localize with Brp, and failed to rescue the *srpk79D* mutant phenotype (Fig. 2-8B, 2-8K and data not shown). This suggests that the common N-terminal domain of SRPK79D-RD, SRPK79D-RD* and SRPK79D-RD*KD is required for the axonal transport of SRPK79D and its co-localization with Brp.

Over-expression of SRPK79D disrupts synaptic Brp and impairs synaptic function

Our data are consistent with a model in which SRPK79D prevents premature assembly of T-bars within axons. This model also suggests that SRPK79D activity must be inhibited locally, at the active zone, in order for synaptic T-bar assembly to proceed. We reasoned that over-expressing SRPK79D might overwhelm the synaptic machinery

that disrupts SRPK79D activity and thereby reveal a role for SRPK79D during T-bar assembly or synaptic function. Here we show that SRPK79D over-expression disrupts the punctate, highly organized appearance of synaptic Brp immunoreactivity (Fig. 2-9A – 2-9D, 2-S5A – 2-S5D). For example, we observed regions where Brp was diffusely organized near the synaptic membrane. These regions encompass areas that would normally contain several individual Brp puncta. We hypothesize that these regions of diffuse Brp reflect either failed T-bar assembly or severely perturbed AZ organization. In addition, we found that SRPK79D over-expression also led to a decrease in total synaptic Brp fluorescence (Fig. 2-9C). This might be consistent with perturbed AZ formation but is also similar to that found in homozygous *srpk79D* mutants (*srpk79D^{atc}*), mutants heterozygous for a null mutation in *brp* (*brp^{69/+}*) and mutants heterozygous for the *brp* null mutation and homozygous for the *srpk79D^{atc}* allele (*brp^{69/+}; srpk79D^{atc}*; Fig. 2-2, 2-7, and data not shown). It should be noted however that the diffuse synaptic Brp staining caused by SRPK79D over-expression is not observed in any of these *srpk79D* or *brp* loss-of-function paradigms. It should be further noted that SRPK79D levels in this over-expression experiment are higher than the SRPK79D levels that are sufficient to rescue the *srpk79D* mutation (Fig. 2-3G – 2-3J, 2-9, 2-S5). SRPK localization was determined in rescue animals expressing relatively low levels of transgene-derived SRPK79D and we believe that this is why we observe normal synaptic architecture and SRPK79D localization in those experiments (Fig. 2-8C – 2-8F). Finally, overexpression of SRPK79D-RD*KD (kinase dead) or SRPK79D-RD (truncated kinase domain) did not cause diffuse Brp staining (data not shown) indicating that the kinase domain is required for this phenotype.

If SRPK overexpression perturbs T-bar assembly or organization, then we might expect a disruption of presynaptic vesicle release. When we assayed synaptic function in larvae over-expressing SRPK we found a dramatic (~50%) decrease in EPSP amplitude along with a modest increase in the average amplitude of spontaneous miniature events (minis, Fig. 2-9F, 2-9G). Estimating the average number of vesicles released per action potential (quantal content; calculated according to the average EPSP/average mEPSP per NMJ) we found that quantal content was severely perturbed. Since synapse function is intact in *srpk79D^{atc}* homozygous animals, *brp^{69/+}* heterozygous animals, and *brp^{69/+}; srpk79D^{atc}* double mutant larvae (see above), the defects caused SRPK79D overexpression are likely a consequence of excess SRPK79D activity at AZs. In addition, overexpression of SRPK79D-RD*KD (kinase dead) or SRPK79D-RD (truncated kinase domain) did not cause a defect in synaptic function (data not shown) indicating that the kinase domain is required for this overexpression phenotype. Finally, it is worth noting that the defects in synaptic function caused by SRPK79D-RD* overexpression are similar to those found in *brp* null mutants, which lack T-bars [Kittel et al. 2006].

Discussion

Here we present the identification and characterization of a novel serine threonine kinase termed "Serine-Arginine Protein Kinase at 79D" (SRPK79D) that co-localizes with the T-bar associated protein Brp in both the axon and at the mature AZ. ATC is one of very few proteins known to localize to T-bars or Ribbon-like structures at the AZ and is the only known kinase to localize to this site [Schmitz et al. 2000, Zhai & Bellen 2004, tom Dieck et al. 2005, Kittel et al 2006, Wagh et al. 2006] (Fig. 2-8). We further provide genetic evidence that SRPK79D functions to represses the premature assembly of T-bars in axons. In particular, we show that loss-of-function mutations in *srpk79D* cause the appearance of T-bar-like protein aggregates throughout peripheral axons and we are able to rule out the possibility that this is an indirect consequence of generally impaired axonal transport (Fig. 2-4, 2-6). The appearance of ectopic T-bars is highly specific since numerous other synaptic proteins and mitochondria are normally distributed in the neuron and are normally trafficked to the presynaptic nerve terminal in the *srpk79D* mutant background (Fig. 2-4A – 2-4L). Thus, SRPK79D appears to have a specific function in repressing T-bar assembly prior to the AZ, consistent with the strong co-localization of SRPK79D protein with Brp and T-bar structures.

Finally, we also uncover a potential function for SRPK79D at the AZ where it is observed to co-localize with Brp. SRPK79D loss of function mutations do not alter the number, density or organization of Brp puncta at the synapse and do not alter synaptic function (Fig. 2-2 and data not shown). This is consistent with a negative regulatory role for SRPK79D during T-bar assembly and indicates that once SRPK79D-dependent repression of T-bar assembly is relieved that active zone assembly proceeds normally.

Overexpression of SRPK79D however severely disrupts neurotransmission. The defect in presynaptic release is correlated with a disruption of Brp puncta organization and integrity. These phenotypes are consistent with a function for SRPK79D as a negative regulator of T-bar assembly and AZ maturation.

SRPK79D is a member of the SRPK family of constitutively active cytoplasmic serine-threonine kinases that target serine-arginine rich domains of SR proteins [Colwill et al. 1996, Koizumi et al. 1999, Yeakley et al. 1999, Nolen et al. 2001]. Thus, it is interesting to postulate what the relevant kinase target might be. Given that SRPK79D and Brp co-localize, an obvious candidate is the Brp protein itself. However, the Brp protein does not have a consensus SR domain and decreasing the genetic dosage of *srpk79D* does not potentiate axonal Brp accumulations that appear upon Brp over-expression[Wagh et al. 2006] (Fig. 7J). As such, Brp may not be the direct target of SRPK79D kinase activity. We hypothesize therefore that SRPK79D co-localizes with Brp and another putative SR protein that is the direct target of SRPK79D kinase activity.

Potential models for SRPK79D-dependent negative regulation of T-bar assembly

The best-characterized role for SRPKs is in controlling the subcellular localization of SR proteins, thereby regulating their nuclear pre-mRNA splicing activity [Graveley 2000]. More recently, SR protein involvement in several cytoplasmic mRNA regulatory roles has been reported [Huang & Steitz 2005, Bedard et al. 2007]. In particular, a phosphorylation-dependent role for SR proteins has been reported in both *Drosophila* and mammalian cell culture [Miron et al. 2003, Blaustein et al. 2005].

It is interesting to speculate that the function of SRPK79D to prevent premature T-bar assembly might be related to the established function of SRPKs and SR-domain

containing proteins during RNA binding, processing and translation [Graveley 2000, Huang & Steitz 2005]. One interesting possibility is that RNA species are resident at the T-bar. In such a scenario, SRPK79D dependent repression of RNA translation could prevent T-bar assembly in the axon and relief of this repression would enable T-bar assembly at the AZ. The continued association of SRPK79D with the AZ could allow regulated control of further T-bar assembly during development, aging and possibly as a mechanism of long-term synaptic plasticity. Several results provide evidence in support of such a possibility. First, local translation has been proposed to control local protein concentration within a navigating growth cone [Wu et al. 2005, Leung et al. 2006]. There is also increasing evidence in support of local translation in dendrites and for the presence of Golgi outposts that could support local protein maturation [Sutton et al. 2006, Ye et al. 2007]. A specific role for RNA binding proteins at the presynaptic AZ is supported by the prior identification of the RIBEYE protein, which is a constituent of the vertebrate ribbon structure. RIBEYE contains a CtBP domain previously shown to bind RNA [Schmitz et al. 2000]. The discovery of a different RNA binding protein (CtBP1) at the ribbon and our description of a putative RNA regulatory protein at the *Drosophila* T-bar further suggest that RNA processing might be involved in the formation or function of these presynaptic electron dense structures [tom Dieck et al. 2005].

In light of these data, we explored the possibility that SRPK79D might participate in translational control related to T-bar assembly. To test this idea we analyzed nerves of mutants for several genes that function in mRNA transport and local protein translation in the *Drosophila* embryo. We first examined mutations in genes that could represent SRPK79D-dependent negative regulators of translation such as *aret (bru)*, *cup*, *pum*, *nos*

and *sqd* [Eldon & Pirrotta 1991, Kraut & Levine 1991, Barker et al. 1992, Keyes & Spradling 1997, Webster et al. 1997, Kindler et al. 2005, Steinhauer & Kalderon 2005], reasoning that the loss of such a translational inhibitor might result in the ectopic synthesis of active zone proteins ultimately leading to a phenotype similar to that observed in *srpk79D* mutants . We also generated genomic deletions for *bru2* and *bru3*. However, we did not find evidence of axonal Brp aggregation in any of these mutants. Next, we assayed mutations previously shown to be required for mRNA transport and local protein synthesis. If necessary for T-bar assembly, these mutations might disrupt synaptic Brp-dependent T-bar formation. These mutations, including *orb*, *vas* and *stau*, have phenotypes at earlier stages of development, but show no defect in synaptic Brp staining [Jack & McGinnis 1990, Christerson & McKearin 1994, Lantz et al. 1994, Tinker et al. 1998, Kindler et al. 2005]. Thus, although these experiments do not rule out a function for SRPK79D in local translation, we have examined mutations in several additional candidates and failed to uncover evidence in support of this model.

Another possibility is that SRPK79D inhibits T-bar assembly through the constitutive phosphorylation-dependent control of a putative SR protein that co-localizes with SRPK79D and Brp within a nascent T-bar protein complex. Upon arrival of this nascent T-bar protein complex at the presynaptic nerve-terminal, T-bar assembly could be initiated in a site-specific manner through the action of a phosphatase that is concentrated at a newly forming synapse. There are several examples of phosphatases that can be localized to sites of intercellular adhesion, some of which have been implicated in the mechanisms of synapse formation and remodeling [Syken et al. 2006]. This model, therefore, proposes that negative regulation of T-bar assembly, via

SRPK79D, is a critical process required for the rapid and site-specific assembly of the presynaptic AZ-associated T-bar structure. Finally, we can not rule out the possibility that SRPK79D normally functions to prevent T-bar super-assembly as opposed to T-bar assembly per se. Consistent with this idea is the observation of T-bar aggregates in axons and prior observation that detached ribbon structures coalesce into large assemblies in vertebrate neurons [Dick et al. 2003].

Controlling the process of synapse assembly through negative regulation

Synapse assembly is a remarkably rapid event. There is evidence that the initial stages of synapse assembly can occur in minutes-to-hours followed by a more protracted period of synapse maturation [Shapira et al. 2003, Buchanan et al. 1998, Sanes & Lichtman 1999, Goda & Davis 2003]. Synapses are also assembled at specific sites. In motoneurons and some central neurons, synapses are assembled when the growth cone reaches its muscle or neuron target [Jontes et al. 2000, Goda & Davis 2003]. However, many central neurons form *en passant* synapses that are rapidly assembled at sites within the growing axon, behind the advancing growth cone [Jontes et al. 2000, Goda & Davis 2003]. Current evidence supports the conclusion that intercellular signaling events mediated by cell adhesion and transmembrane signaling specify the position of the nascent synapse [Davis et al. 1997, Jontes et al. 2000, Shen et al. 2004]. The subsequent steps of presynaptic AZ assembly remain less clear. Calcium channels and other transmembrane and membrane-associated proteins appear to be delivered to the nascent synaptic site via transport vesicles that fuse at the site of synapse assembly [Ahmari et al. 2000, Zhai et al. 2001, Shapira et al. 2003]. It has been proposed that cytoplasmic scaffolding molecules then gradually assemble at the nascent synapse by linking to the

proteins that have been deposited previously [Shapira et al. 2003]. This model, assumes, however, that the protein-protein interactions between the numerous scaffolding molecules that comprise the presynaptic particle web, do not randomly or spontaneously occur in the cytoplasm prior to synapse assembly. What prevents these scaffolds from spontaneously assembling in the small volume of an axon, prior to synapse formation at the nerve terminal and between individual *en passant* synapses? Currently, nothing is known about how premature scaffold assembly is prevented. We propose that our studies of *srpk79D* identify one such mechanism of negative regulation that prevents premature, inappropriate, assembly of a presynaptic protein complex. We further propose that such a mechanism of negative regulation, when relieved at a site of synapse assembly, could contribute to the speed with which presynaptic specializations are observed to assemble.

Figures

Figure 2-1. Brp accumulates in *srpk79D* mutant nerves.

(A) The *srpk79D* gene region is shown including the *srpk79D^{atc}* transposon insertion site and deleted regions in mutants used for genetic analyses (black bars). Gene loci for *srpk79D* and the adjacent *Csp* gene are shown in blue. (B-J) Immunofluorescence images of larval nerves demonstrating large Brp accumulations in *srpk79D* loss-of-function mutants. Each image shows a section of a single larval nerve, photographed at the same relative position approximately 100µm from where the nerve exits the CNS. Each nerve contains approximately 85 total axons, including approximately 35 motor axons. Images are shown at two exposures. Images in (B,E,H) and (C,F,I) were taken at an exposure where small, infrequent anti-Brp puncta could be resolved in wild type nerves. This resulted in over-exposure of the Brp puncta in *srpk79D* mutant nerves. Images (D,G,J) are identical to (B,E,H and C,F,I) except taken at a lower exposure such that no puncta are found in wild type and the puncta intensities are not saturated in the *srpk79D* mutant. (K) Total Brp fluorescence integrated over the nerve area is dramatically increased with *srpk79D* disruption, whereas loss of *Csp* does not increase nerve Brp levels. Each bar graph represents data collected from a total of 30 nerves from 12 different larvae. (L) Cumulative frequency plots of individual Brp punctum fluorescence intensities are shifted toward larger values with *srpk79D* loss-of-function (gray and blue lines representing *srpk79D^{atc}* and *srpk79D^{atc}/Df* respectively are shifted to the far right while other genotypes are clustered to the left). Each curve represents data collected from a total of 30 nerves from 12 different larvae. Sample size for wild type, *srpk79D^{atc}/+*, *srpk79D^{atc}*, *srpk79D^{atc}/Df* and *srpk79D^{atc}/Csp^{XI}* = 479, 1715, 3387, 3718 and 2714

respectively. Brp = anti-Bruchpilot, HRP = anti-horseradish peroxidase. Significance is indicated according to the following: * = $p < 0.05$, ** = $p < 0.01$, *** = $p < 0.001$; student's t-test. Scale bar = $10\mu\text{m}$.

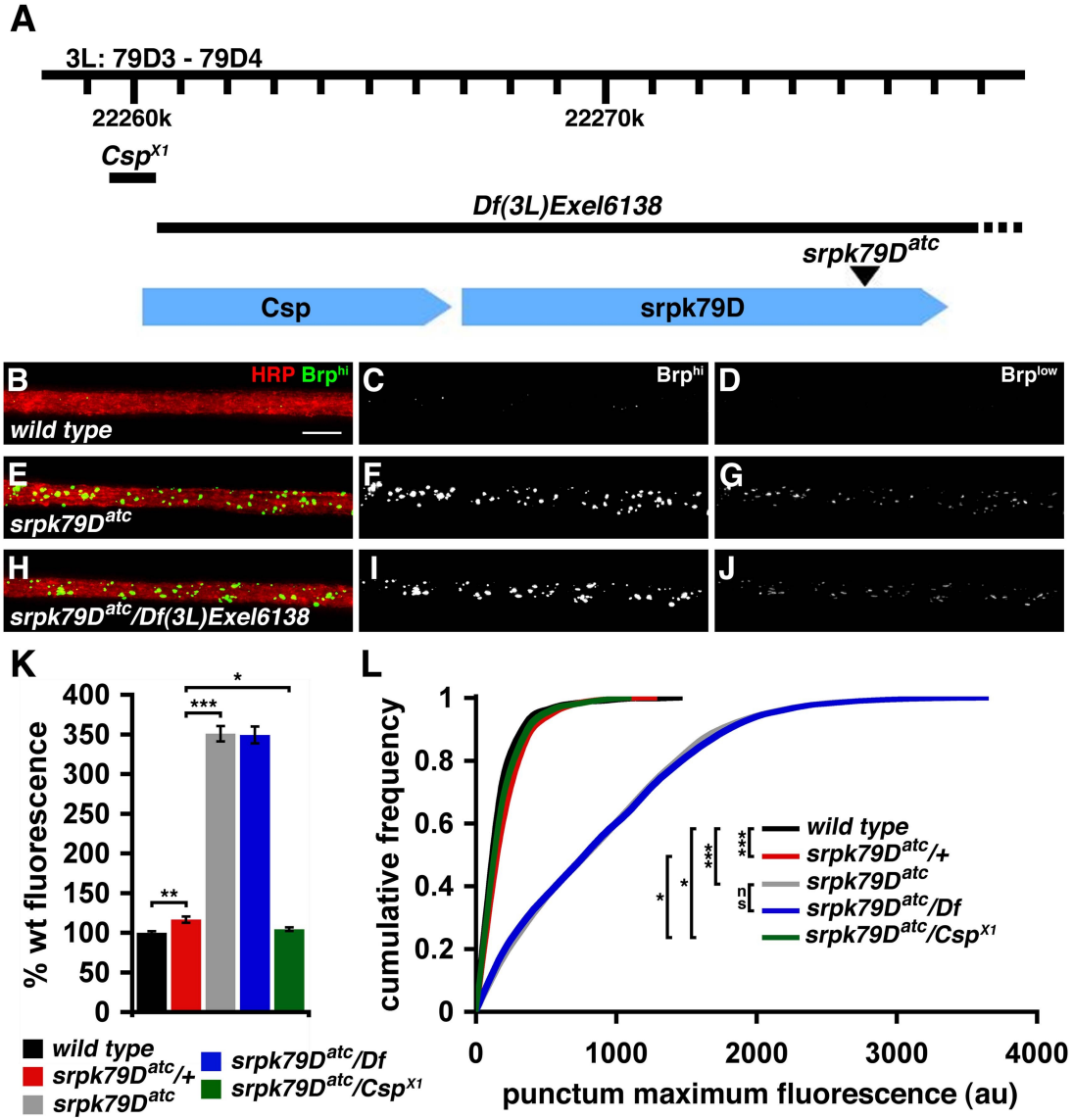


Figure 2-2. Synaptic Brp deficit in *srpk79D* mutants.

(A-D) Immunofluorescence images of *wild type* and *srpk79D^{atc}* mutant NMJ reveal a synaptic Brp deficit in *srpk79D^{atc}* mutants. NMJs are stained with anti-HRP (red) to label the presynaptic membrane and anti-Brp (green). Larvae in *wild type* and *srpk79D^{atc}* were stained in the same reaction tube and imaged identically. (E) The total synaptic Brp fluorescence is decreased in *srpk79D^{atc}* mutants. Each bar graph represents data collected from a total of 30 synapses from 9 different larvae (F) Cumulative frequency plots of synaptic Brp puncta fluorescence intensities are shifted toward smaller values with *srpk79D* loss-of-function. Each curve represents data collected from 30 synapses from 9 different larvae. n for *wild type*, *srpk79D^{atc}* and *srpk79D^{atc}/Df* = 6554, 4713 and 5952 respectively. (G, H) Disruption of *srpk79D* affects neither synaptic Brp puncta number (G) nor synaptic bouton number (H). Each bar graph in (G) and (H) represents data collected from a total of 38 synapses taken from 15 different larvae. Scale bar = 10 μ m.

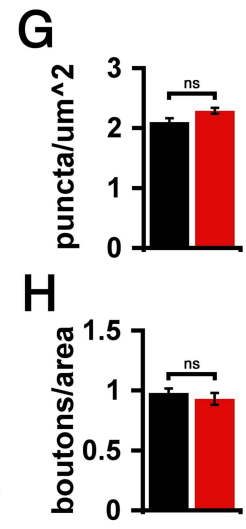
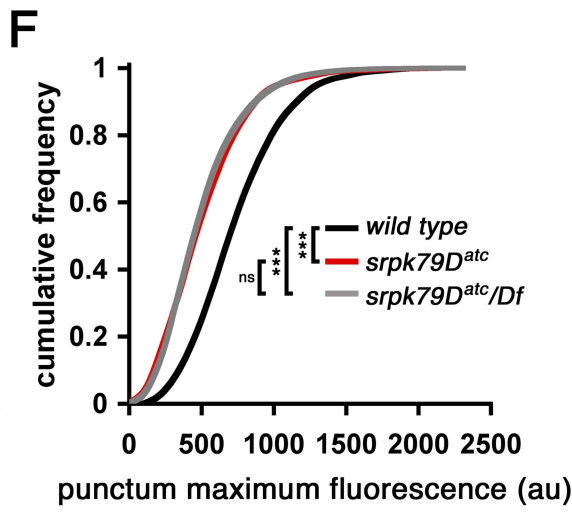
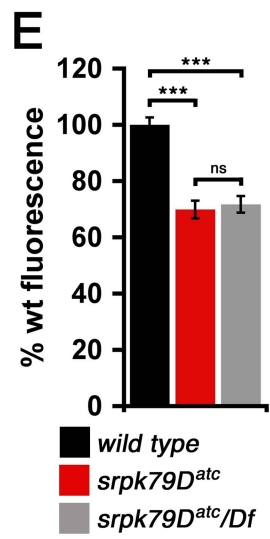
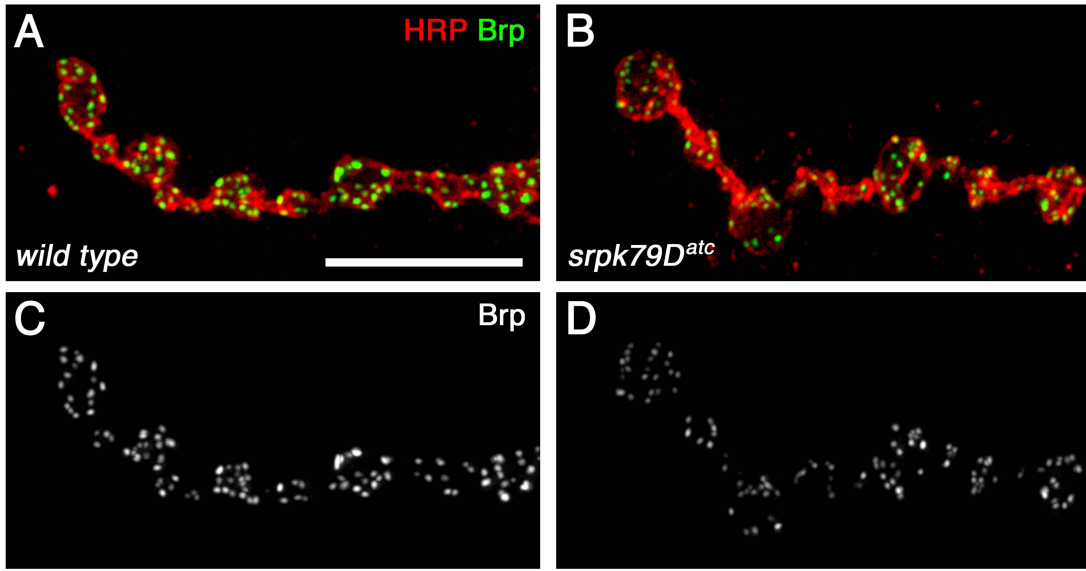


Figure 2-3. SRPK79D functions in neurons to prevent Brp accumulation.

(A,B) Whole mount *in situ* hybridizations demonstrate that *srpk79D* is widely expressed but is enriched in the CNS. Anterior is to the left. (C,D) Immunofluorescence images of a control nerve (C) and a nerve expressing *srpk79D*-specific dsRNA (UAS-*srpk79D*^{RNAi}) in neurons (D). Expression of dsRNA causes accumulation of Brp puncta. (E,F) Total Brp fluorescence is increased and cumulative frequency plots are shifted toward larger values when *srpk79D*^{RNAi} is expressed in neurons, but not when it is expressed in glia using the glia-specific Repo-GAL4 driver. Each bar graph and curve in (E) and (F) represents data collected from a total of 30 nerves from 9 different larvae. In (F), n for C155/+, C155/+;;UAS-*srpk79D*^{RNAi}/+, Repo/+, Repo/UAS-*srpk79D*^{RNAi} = 1034, 2451, 893, 862. (G-J) Expression of a Venus-tagged *srpk79D* transgene (UAS-*v-srpk79D-rd**) rescues Brp accumulations in *srpk79D* mutant nerves. (G-H) Nerves are stained with anti-Brp and imaged identically. Brp accumulations are present in the *srpk79D* mutant (G) and these accumulations are less intense following rescue of the *srpk79D* mutant with the UAS-*srpk79D* transgene (H). (I-J) Quantification of Brp fluorescence intensity (I) and puncta intensities (J), comparing control (C155 /+), *srpk79D* mutant (C155/+;*srpk79D*^{atc}) and rescue animals (C155/+; UAS-*v-srpk79D-rd*(28)*/+;*srpk79D*^{atc}). Each bar graph and curve in (I) and (J) represent data collected from a total of 36 nerves from 9 different larvae. In (J), n for C155/+, C155/+;;*srpk79D*^{atc}, C155/+;UAS-*v-srpk79D-rd*(28)*/+;*srpk79D*^{atc} = 2452, 2696, 3645. Scale bar = 10µm.

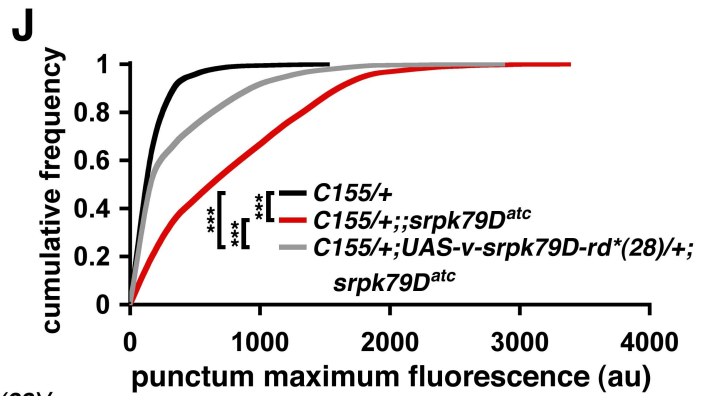
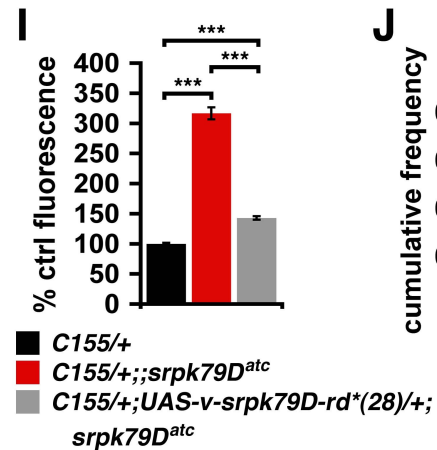
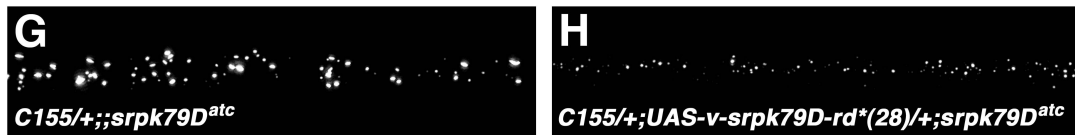
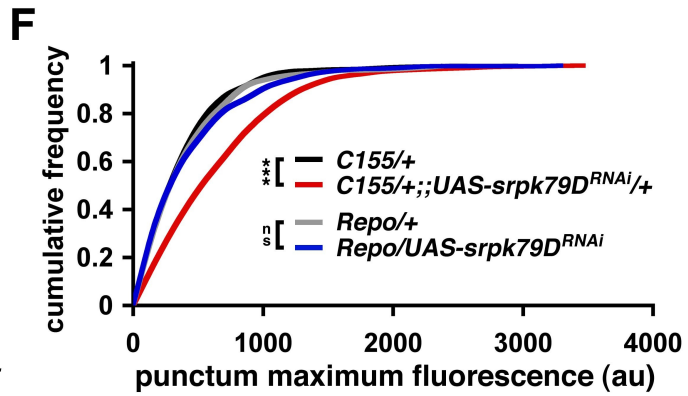
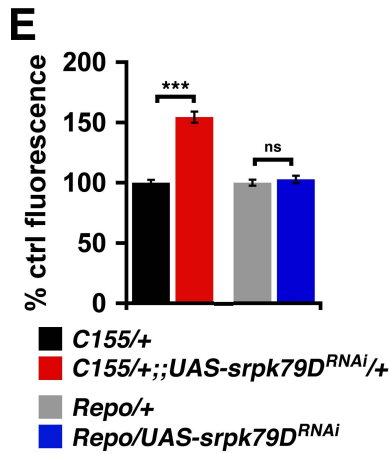
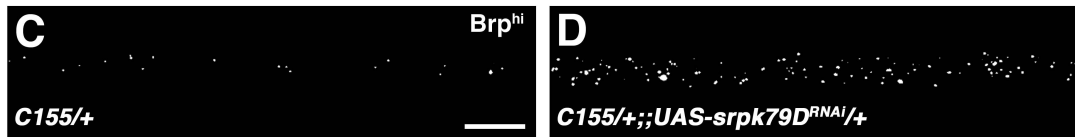
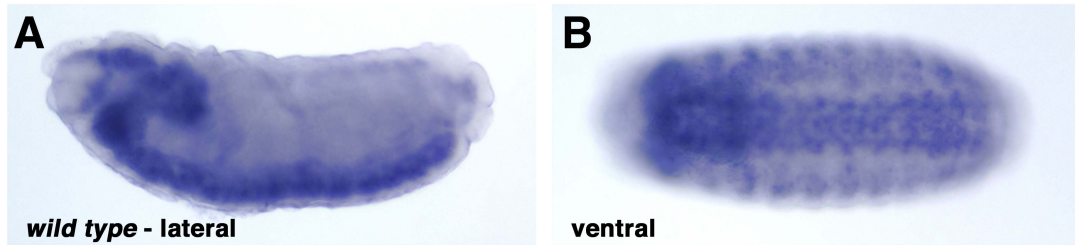


Figure 2-4. Kinesin-/Dynein-based axonal transport is intact in *srpk79D* mutants.

(A-L) Immunofluorescence images of *wild type* and *srpk79D* mutant nerves demonstrating the distribution of Bruchpilot (Brp; A,B) the synaptic vesicle proteins Synaptotagmin 1 (Syt; C,D) and Cysteine String Protein (CSP; E,F), mitochondria (mitoGFP; G,H), the peri-AZ protein Dap160/Intersectin (Dap160; I,J), and the AZ protein Liprin-alpha (Lip- α ; K,L). Image exposures were selected such that small puncta could be visualized in the wild type controls, corresponding to a 'high exposure' in Figure 1. Wild type and *srpk79D* mutants were stained in the same reaction tube and imaged identically for each antibody. (M,N) Reducing *kinesin heavy chain* (*Khc*^{8/+}) or *immaculate connections* (*imac*^{170/+}) in the *srpk79D* mutant background does not enhance the *srpk79D* mutant phenotype. Each bar graph in (M) and curve in (N) represents data collected from a total of 30 nerves from 9 different larvae. In (N), n = 1040, 2928, 2560, 3240 for wild type, *srpk79D^{atc}*, *Khc*^{8/+}; *srpk79D^{atc}* and *imac*^{170/+}; *srpk79D^{atc}* respectively. Scale bar = 10 μ m.

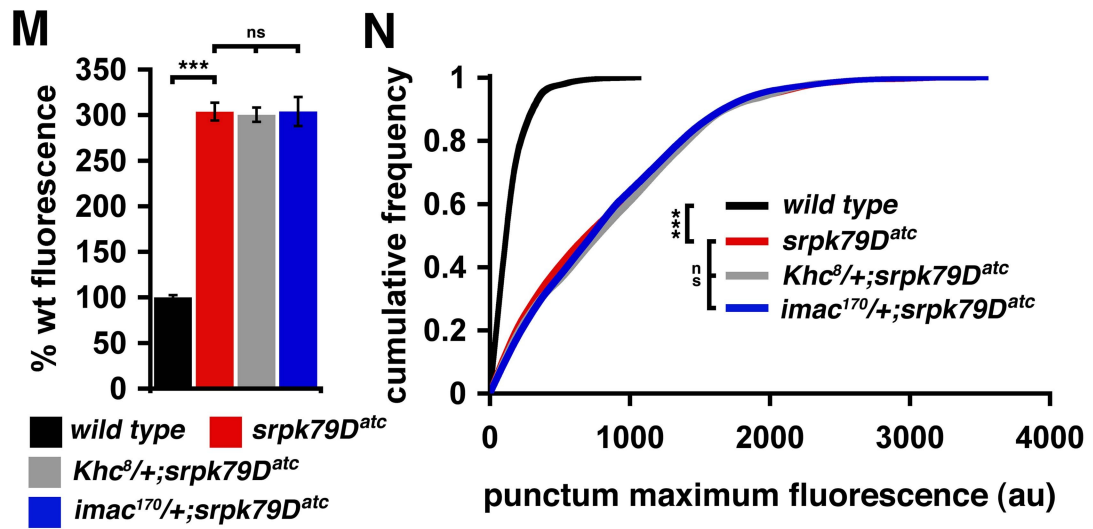
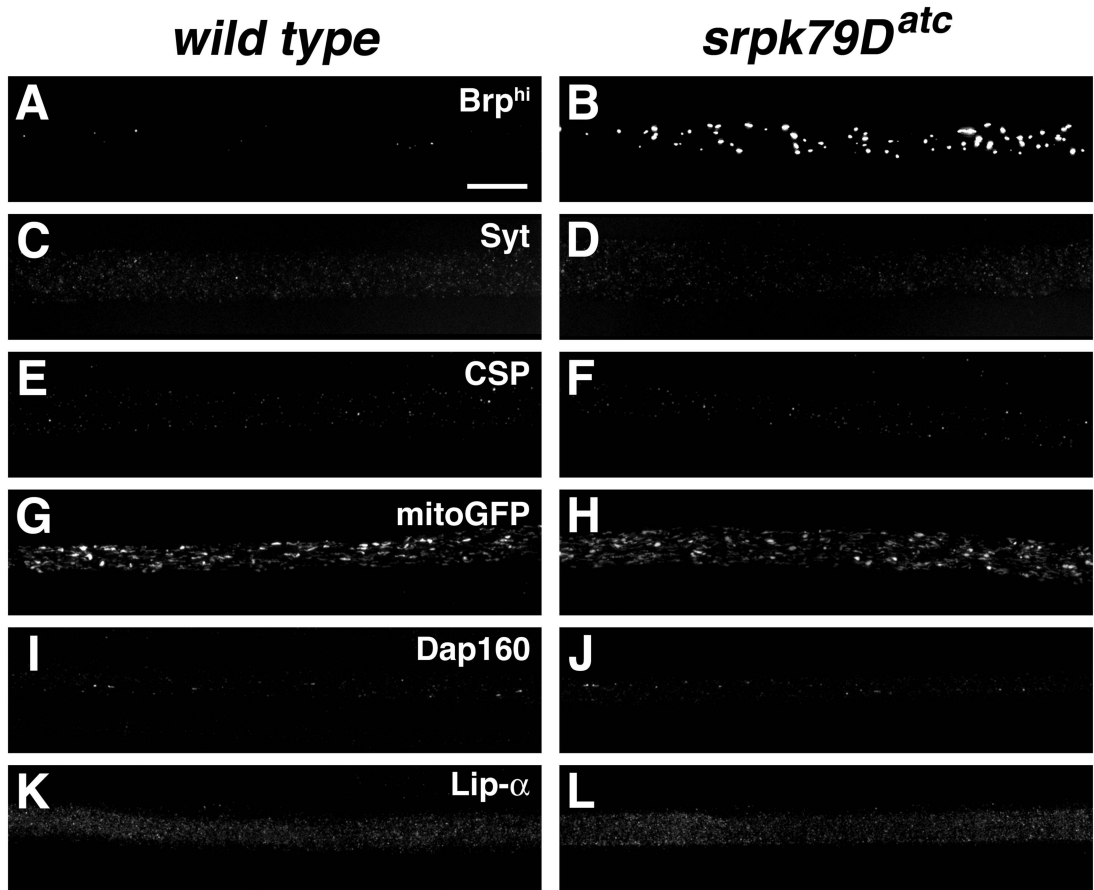


Figure 2-5. Comparison of synaptic and axonal Brp assemblies in *wild type* and *srpk79D* mutant animals.

(A-D) Immunofluorescence images of *wild type* and *srpk79D* mutant nerves and synapses. Insets in (C) and (D) show the shape of the nerve terminal arborization at lower magnification based upon co-staining with anti-Hrp. (E) Cumulative frequency plots of individual Brp puncta fluorescence intensities. Each curve represents data collected from a total of 18 nerves or synapses from 9 larvae. Arrowheads on the x-axis in (E) indicate the average maximum punctum fluorescence intensity for each genotype (indicated by arrowhead color). Scale bars = 10 μ m.

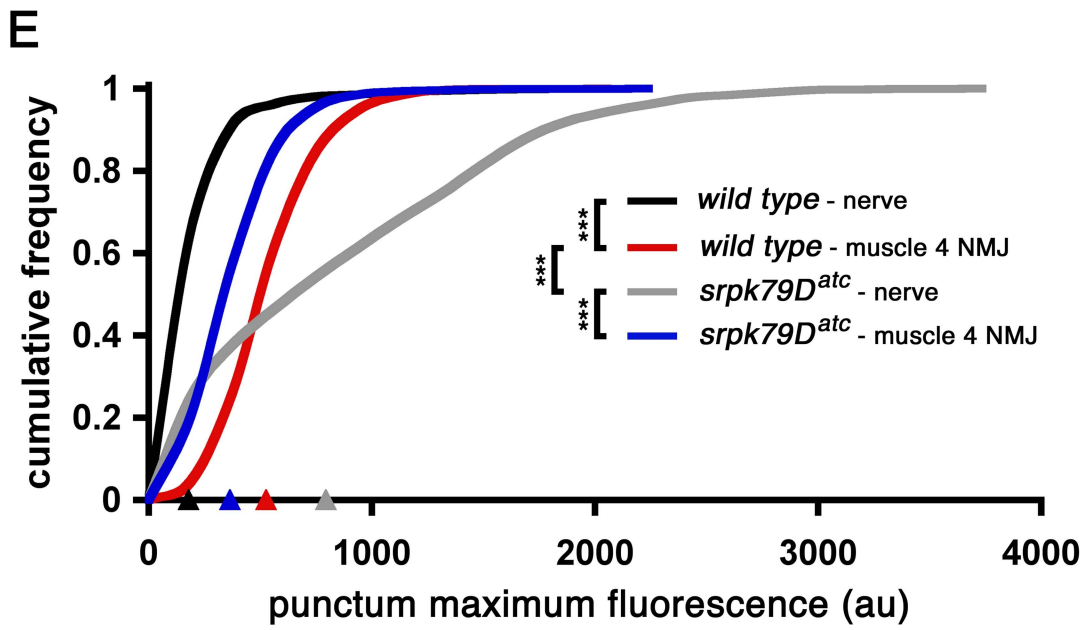
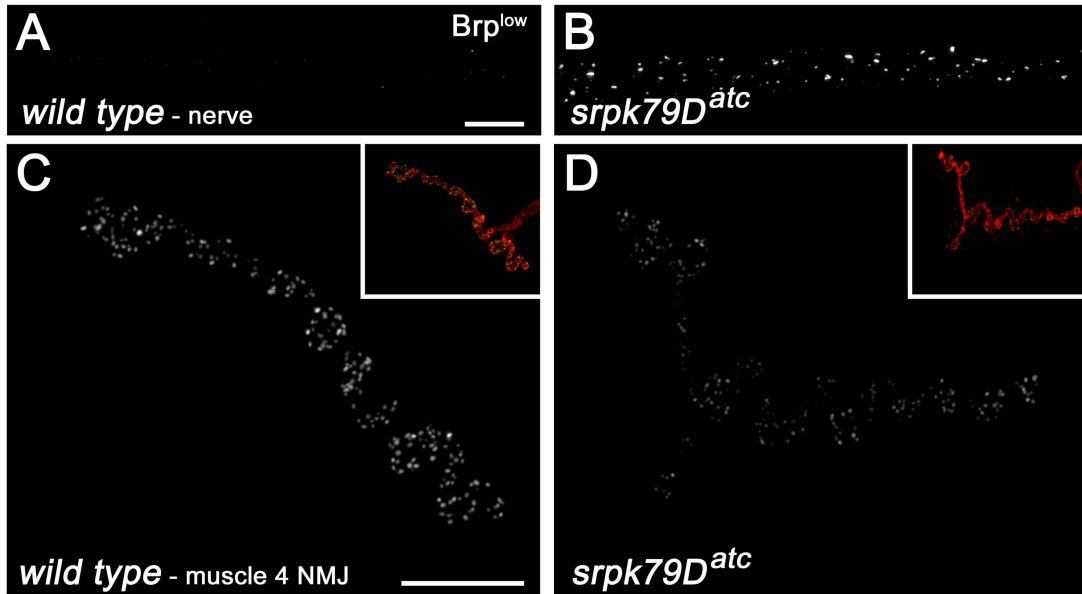


Figure 2-6. T-bar super-assemblies are found in *srpk79D* mutant axons.

(A,B) Electron micrographs of *srpk79D* mutant motor axons showing large, electron-dense structures that are never found in *wild type* axons. (C) Magnified image of region boxed in B highlighting an accumulation that is particularly reminiscent of a super-assembly of T-bars. (D) A wild type synaptic T-bar at the same magnification for comparison to the image in (C).

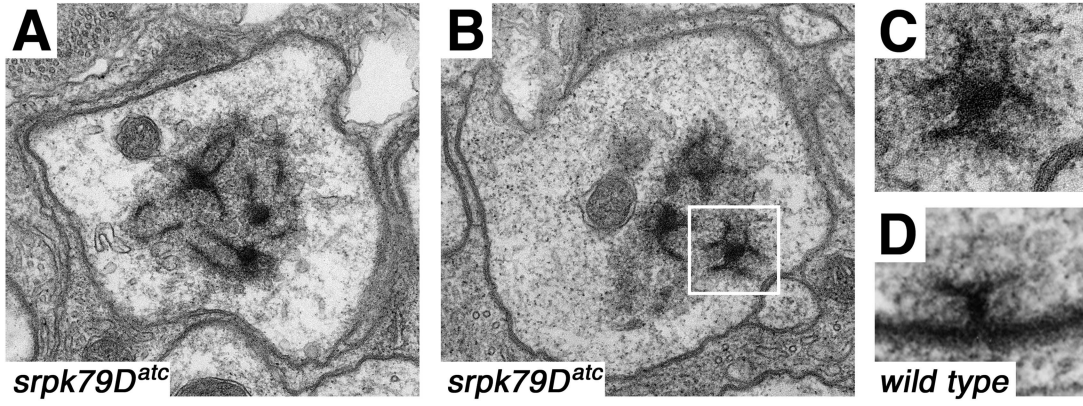


Figure 2-7. Brp accumulation in *srpk79D* mutants is not due to increased Brp expression.

(A,B) Immunofluorescence images of *wild type* and *srpk79D* mutant nerves. (C) Similar Brp accumulations appear when GFP-Brp is overexpressed in motor neurons using the motoneuron-specific GAL4 driver *OK371-GAL4*. (D) Brp accumulations persist in *srpk79D* mutants when one copy of *brp* is deleted by placing a heterozygous *brp^{69/+}* mutation in the homozygous *srpk79D* mutant background. (E,F) Immunofluorescence images of *wild type* and *srpk79D* mutant muscle 4 NMJ stained with anti-Brp. (G) Synaptic Brp is increased following GFP-Brp overexpression. (H) Removal of one copy of *brp* (*brp^{69/+}*) in a homozygous *srpk79D* mutant background causes a further decrease in synaptic Brp levels compared to *srpk79D* mutants alone, but does not cause altered distribution of Brp immunoreactivity. (I) Quantifications of total Brp fluorescence for each indicated genotype normalized to *wild type*. Each bar graph represents data collected from a total of 29 synapses from 14 different animals. (J) Total Brp fluorescence is increased in *srpk79D^{atc/+}* heterozygotes (*OK371/+; srpk79D^{atc/+}*) and when Brp is overexpressed in motor neurons (*OK371/+; UAS-g-brp*). An additive effect is seen when these two perturbations are combined (*OK371/+; UAS-brp/srpk79D^{atc}*). In all cases total synaptic anti-Brp fluorescence is significantly less than seen in *srpk79D* mutants (*srpk79D^{atc}*). Each bar graph represents data collected from a total of 32 synapses from 8 different larvae. Scale bars = 10µm.

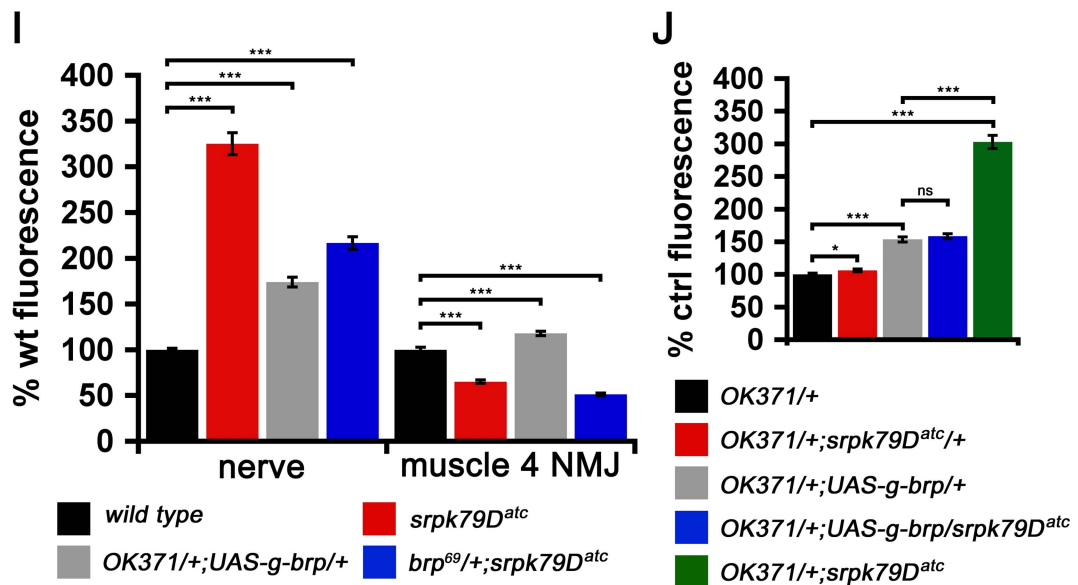
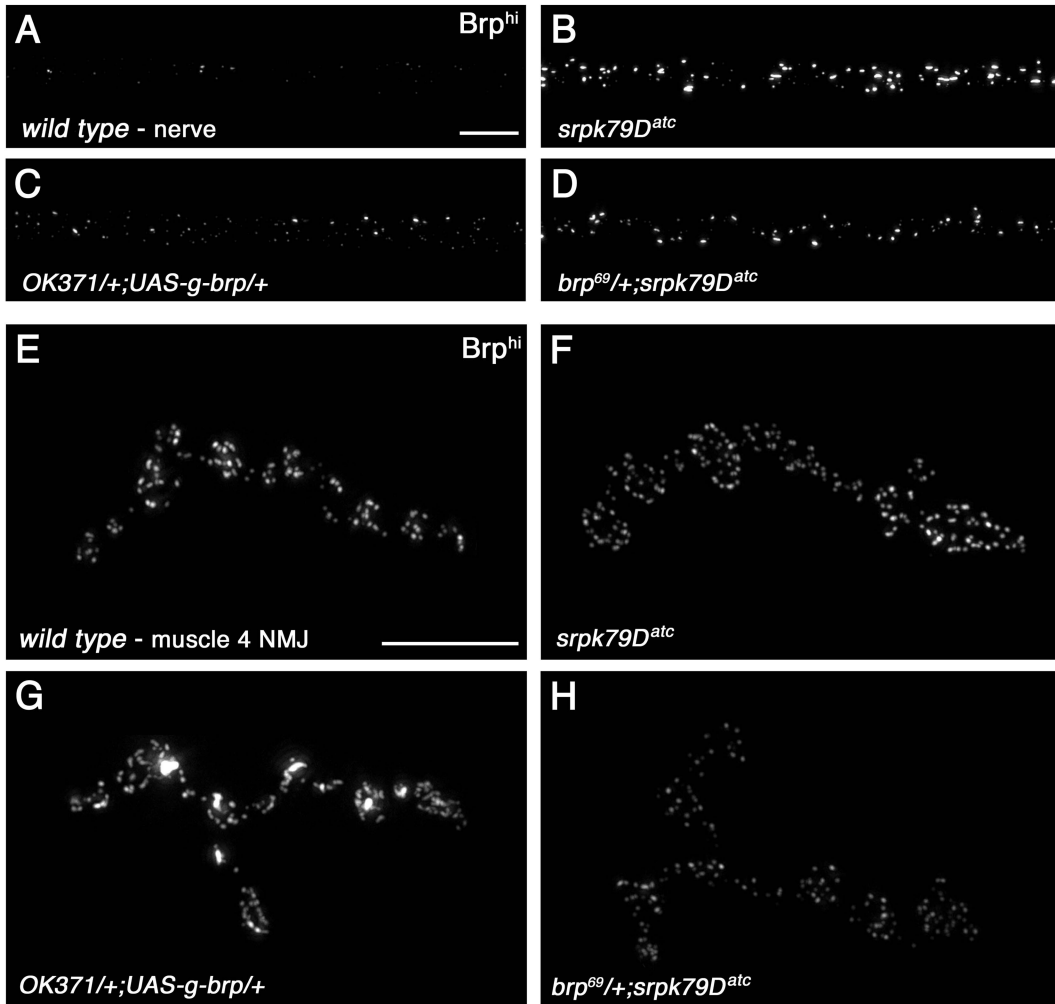
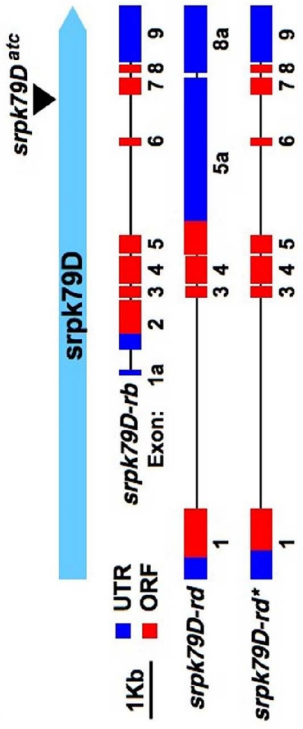
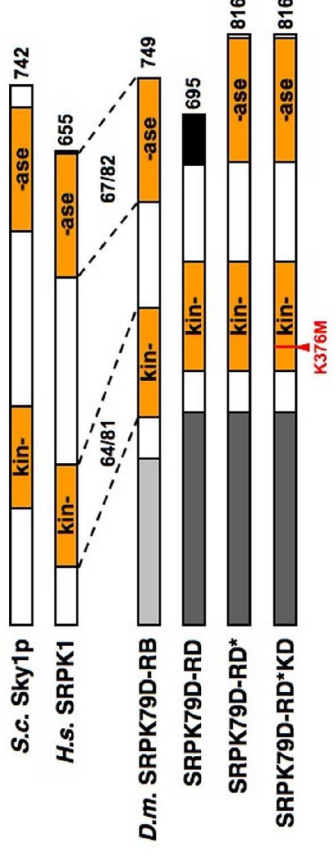
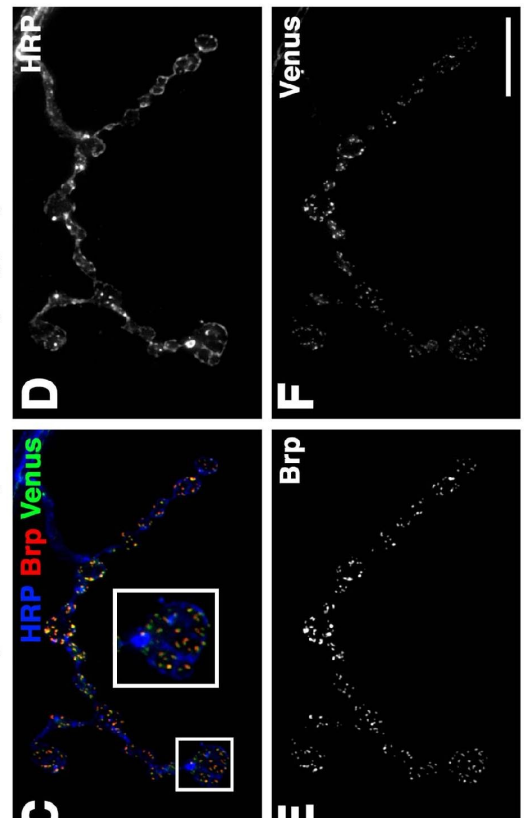
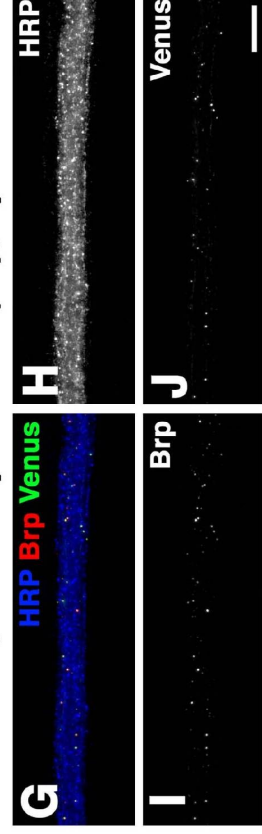


Figure 2-8. SRPK79D kinase activity is necessary and the SRPK79D N-terminus directs targeting.

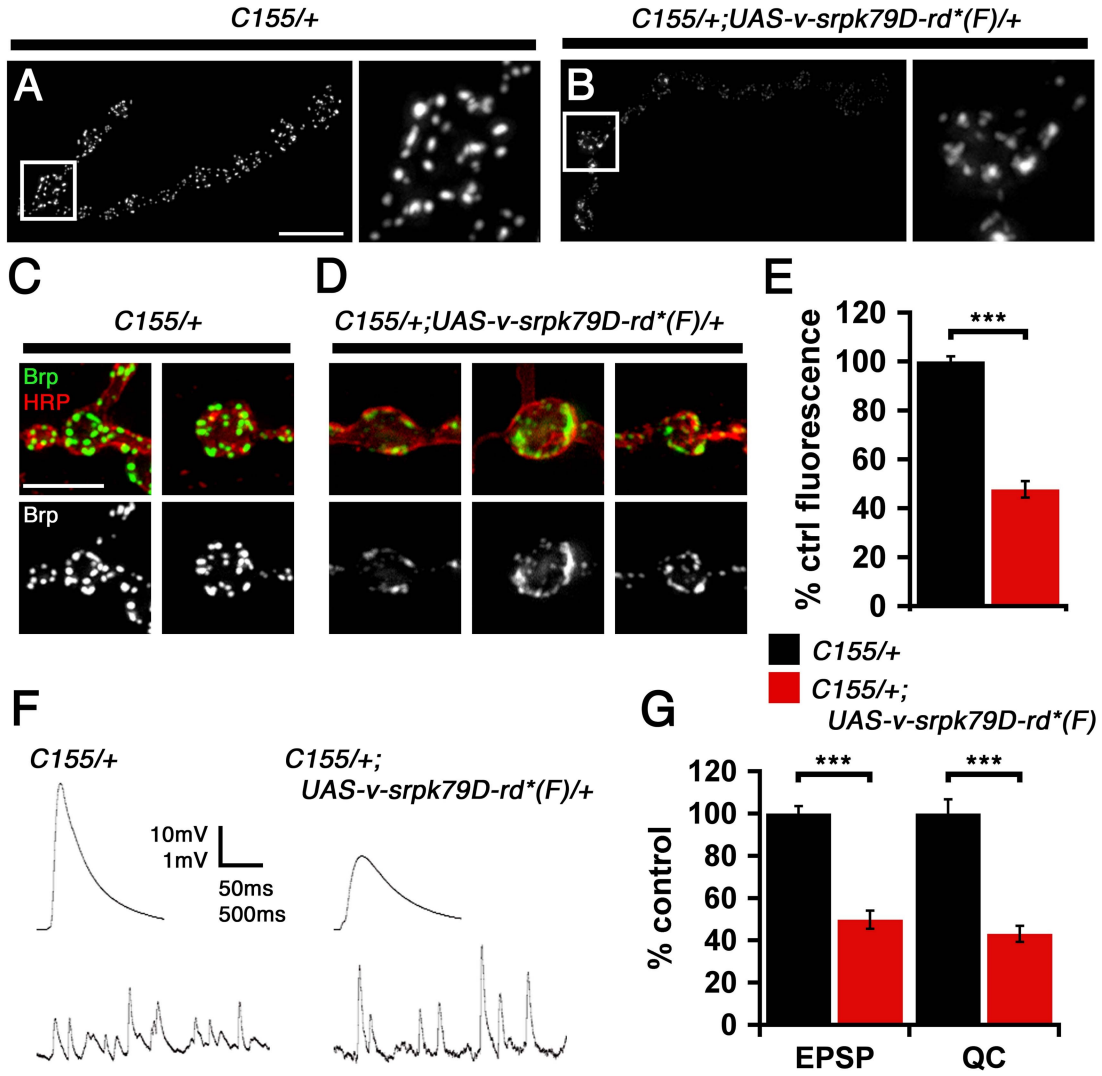
(A) A schematic of two previously cloned *srpk79D* transcripts (*srpk79D-rb* and *srpk79D-rd*) [Stapelton et al. 2002]. *srpk79D-rd* results from read-through of predicted splice sites in exons 5 and 8. We generated the transcript conforming to the predicted splicing pattern of exons 5 and 8 is also shown (*srpk79D-rd**). We have since confirmed the existence of this transcript by reverse-transcriptase PCR. (B) A schematic of yeast Sky1p and human SRPK1 protein domain structures as well as domain structures for the predicted *srpk79D* protein products (SRPK79D-RB, SRPK79D-RD and SRPK79D-RD*). Alternative exon usage results a unique SRPK79D-RB N-terminus (light gray), whereas SRPK79D-RD and SRPK79D-RD* use the same N-terminus (dark gray). The splicing pattern employed in SRPK79D-RD leads to a truncated kinase domain relative to SRPK79D-RB* and SRPK79D-RD. SRPK79D-RD*KD contains a missense mutation at position 376 (K376M) that targets the predicted ATP binding site. Numbers indicate the percent amino acid identity/similarity of the SRPK79D kinase domain to that of human SRPK1. (C-F, I-J) Immunofluorescence images of synapses and nerves respectively demonstrate near perfect co-localization between Brp and Venus-SRPK79D-RD* in both the NMJ (C-F) and in the axons (G-J). (K) Table indicating Brp co-localization and ability to rescue axon Brp accumulation phenotype of the *srpk79D* gene products indicated in (A) and (B). *S.c.* = *Saccharomyces cerevisiae*, *H.s.* = *Homo sapiens*, *D.m.* = *Drosophila melanogaster*, Scale bars = 10µm. See also Supplemental Discussion relevant to this annotation.

A**B****C155/+;UAS-v-srpK79D-rd*(28);srpk79D^{atc}****C155/+;UAS-v-srpK79D-rd*(28);srpk79D^{atc}****K**

	Brp	
	Co-localization	Rescue
SRPK79D-RB	-	-
SRPK79D-RD	+	-
SRPK79D-RD*	+	+
SRPK79D-RD*KD	+	-

Figure 2-9. SRPK79D over-expression disrupts synaptic Brp and impairs synapse function.

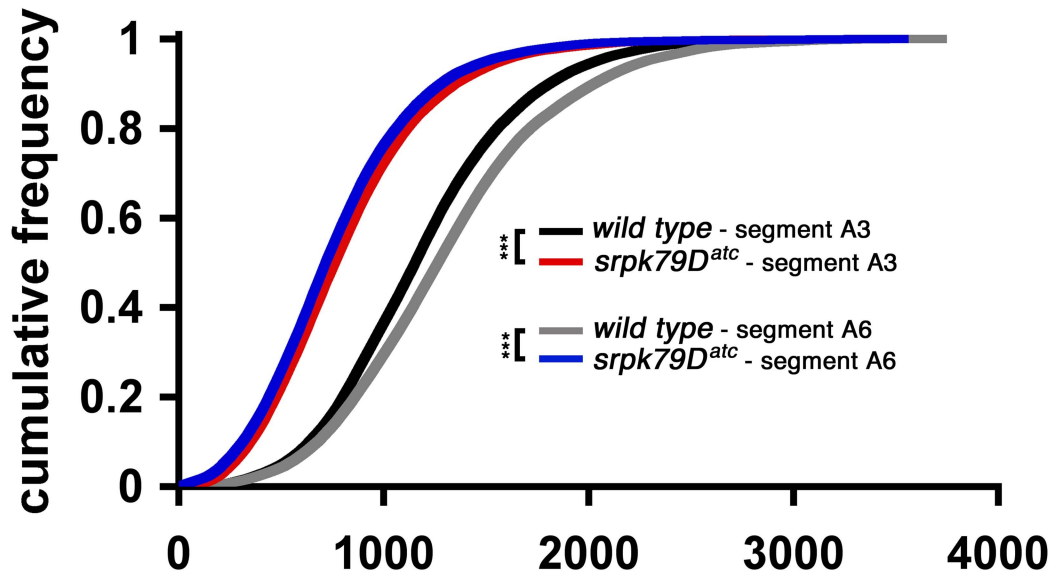
(A,B) Example muscle 4 NMJ and individual bouton from control (*C155/+*) and SRPK79D-RD* overexpressing larvae demonstrating diffuse Brp staining and reduced total Brp fluorescence. Image offset and gain in (A) and (B) are identical (C) Example of type-1b boutons from control animals demonstrating typical punctate anti-Brp staining (green) and anti-HRP staining (red) to elucidate the nerve terminal membrane. (D) Examples of diffuse Brp staining observed at type-1b boutons within the NMJ of an SRPK79D over-expressing animal. Image offset and gain in (C) and (D) are identical. (E) SRPK79D-RD* over-expression causes a decrease in total synaptic Brp fluorescence. (F) Over-expression of SRPK79D-RD* causes a highly significant decrease in EPSP amplitude. There is a trend toward an increase in the average amplitudes of spontaneous miniature events comparing SRPK79D-RD* overexpressing animals to wild type ($p=0.06$), representative mEPSPs are shown. (G) Quantification of average EPSP amplitude and quantal content in SRPK79D-RD* over-expressing larvae show a greater than 50% decreases in both measures relative to *control*. *C155/+* and *C155/+;UAS-v-srpk79D-rd*(F)/+* bar graphs represent data collected from a total of 15 synapses from 6 different larvae and 12 synapses from 5 different larvae respectively. Scale bar in (A) = 10 μ m Scale bar in (C) = 5 μ m.



Supplemental Figure 2-1. Analysis of synaptic Brp levels in anterior and posterior segments from *wild type* and *srpk79D* mutants.

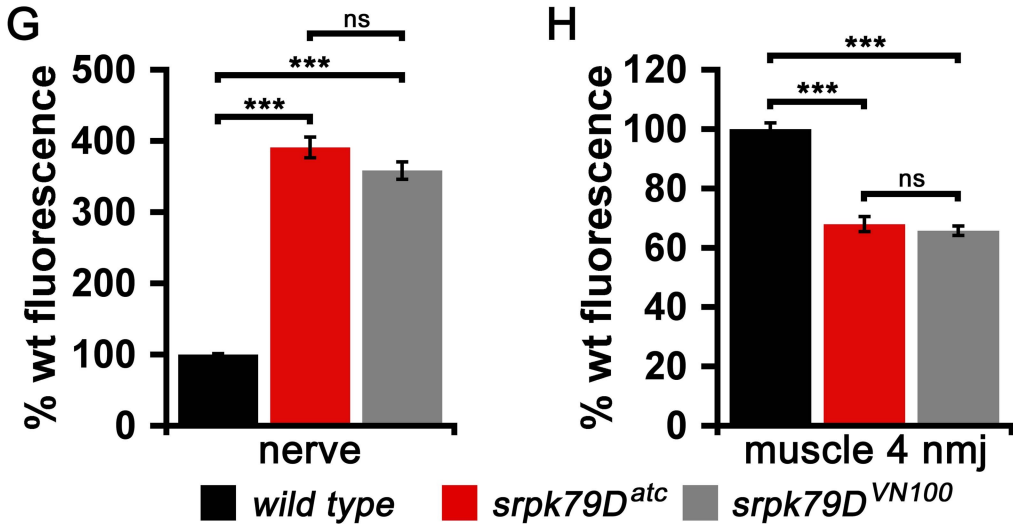
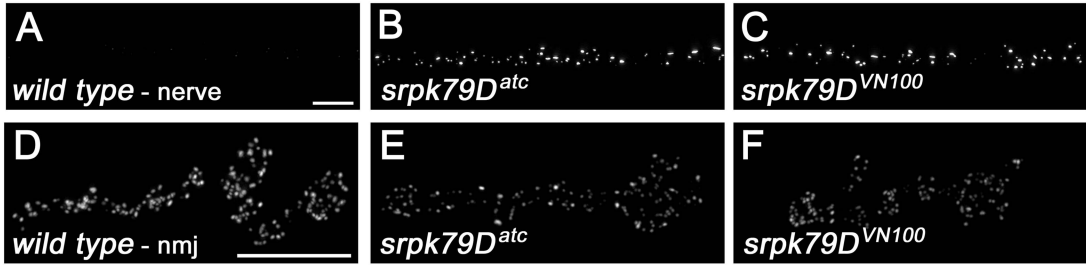
(A) Cumulative frequency plots of individual muscle 4 NMJ Brp puncta maximum pixel intensities from wild type abdominal segment A3 (black curve), *srpk79D^{atc}* segment A3 (red curve), wild type segment A6 (grey curve) and *srpk79D^{atc}* segment A6 (blue curve). There is a slight, though statistically significant, increase in synaptic Brp puncta intensity in wild type segment A6 (posterior) compared to A3 (anterior). In homozygous *srpk79D^{atc}* mutants there is a smaller difference comparing anterior and posterior segments. In conclusion, there is a large decrease Brp synaptic intensity in the mutant compared to *wild type*, and this is not dramatically affected by the position of the NMJ along the anterior-posterior axis. Each curve represents data collected from synaptic arbors of a total of 36 synapses from 18 larvae. n=4657, 3518, 6134, and 4638 respectively. * = p<0.05, ** = p<0.01, *** = p<0.001, Mann-Whitney U Test.

A



Supplemental Figure 2-2. Analysis of an additional *srpk79D* mutation.

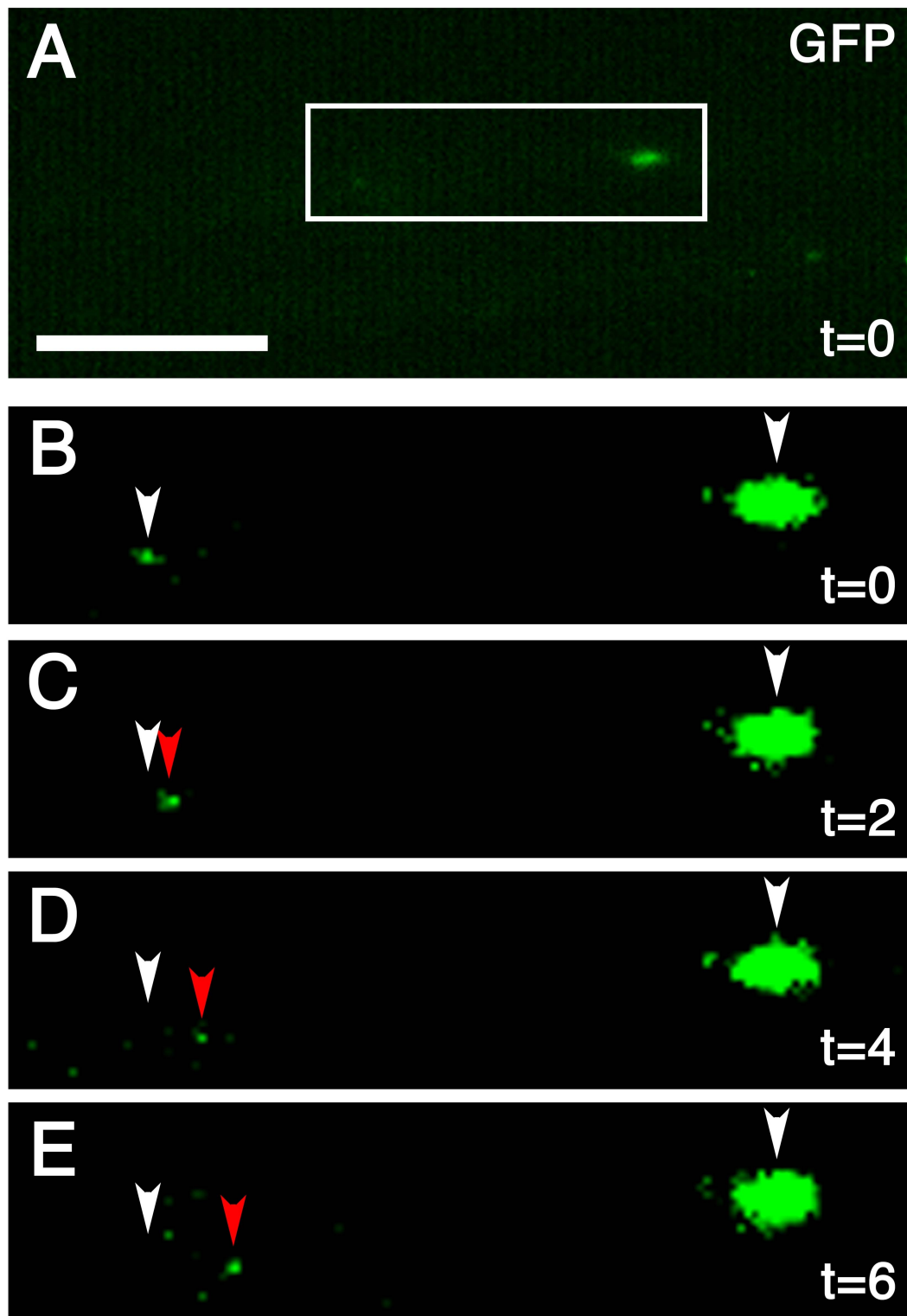
(A-C) Representative immunofluorescence images of individual larval nerves stained with anti-Brp antibody from *wild type* (A), *srpk79D^{atc}* (B), and *srpk79D^{VN100}* (C) larvae. (D-F) Representative immunofluorescence images of muscle 4 NMJs stained with anti-Brp antibody from *wild type* (D), *srpk79D^{atc}* (E), and *srpk79D^{VN100}* (F) larvae. (G,H) Bar graphs showing average (+/- SEM) nerve (G) and muscle NMJ (H) staining intensities. The increases in nerve staining and decreases in synaptic NMJ in the two *srpk79D* mutant conditions are both highly statistically significant compared to *wild type* and statistically indistinguishable from each other. Each bar represents data taken from 24 synapses from 12 larvae. *** = $p < 0.001$, student's t-test. Scale bars = 10 μ m.



Supplemental Figure 2-3. Direct observation of Brp transport.

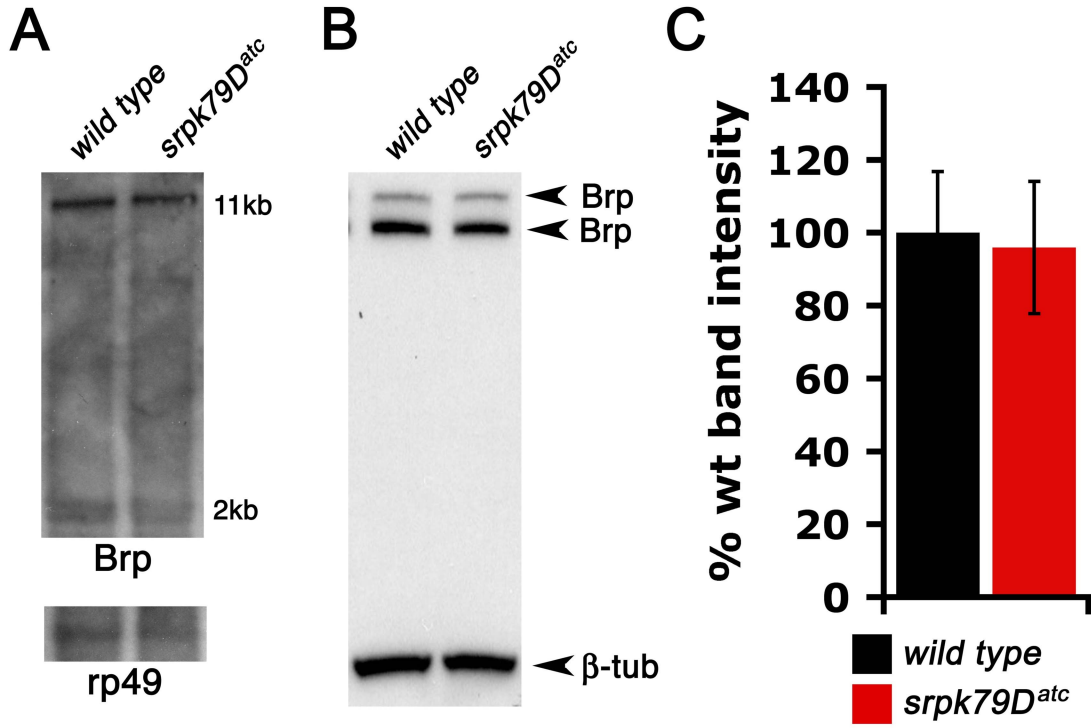
(A) Live GFP fluorescence image of nerves from a *srpk79D^{atc}* mutant larvae expressing GFP-tagged Brp in motoneurons at time=0 seconds. Several small and large GFP-Brp puncta are apparent. Scale bar = 5 μ m. (B-E) a time series (t=0 to t=6 seconds) of upper-left boxed region in (A) demonstrating a motile small BRP punctum and an immobile large BRP aggregate. In (B-E), white arrows indicate the GFP-Brp punctum/aggregate starting point at the beginning of the time series. Red arrows highlight the new position of the motile punctum in each frame. In these experiments we sought to directly assess Brp transport in *srpk79D^{atc}* mutants through live imaging of *srpk79D^{atc}* mutant larval nerves expressing a GFP-tagged brp cDNA in motoneurons [Wagh et al. 2006] (OK371/+;UAS-g-brp, *srpk79D^{atc}/srpk79D^{atc}*). A similar method was used previously to observe GFP-tagged synaptotagmin transport [Miller et al. 2005]. In our experiments, a variety of GFP-Brp species were observed including small puncta and large accumulations. The majority of small GFP-Brp puncta were found to be motile with individual puncta exhibiting anterograde and/or retrograde transport during a given imaging epoch. The average rate of small GFP-Brp puncta transport was 0.08 +/- 0.009 μ m/s (avg +/- SEM). While this rate is somewhat slower than values previously reported for the transport of GFP-tagged Syt, it falls within the range of reported values [Miller et al. 2005]. In contrast, large GFP-Brp accumulations were generally immotile (as shown here). Occasionally, a large accumulation was observed to alternately exhibit anterograde and then retrograde transport. However, total displacement was never more than 0.3 microns (data not shown).

OK371/+;UAS-g-brp,srpk79D^{atc}/srpk79D^{atc}



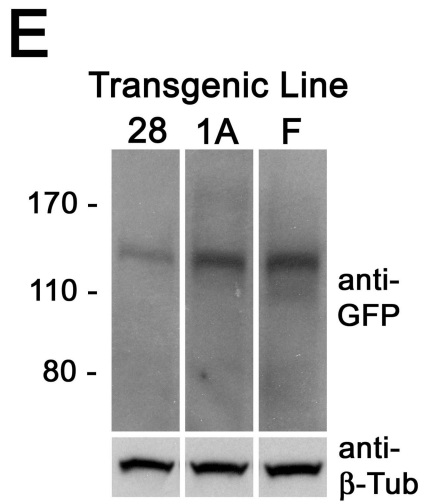
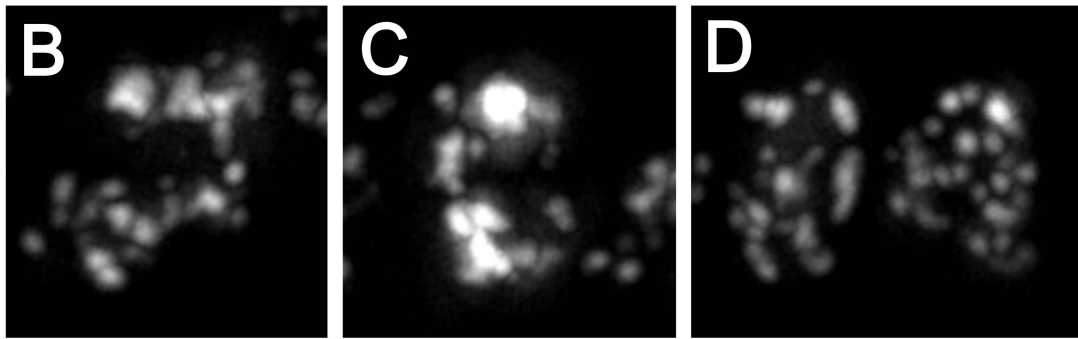
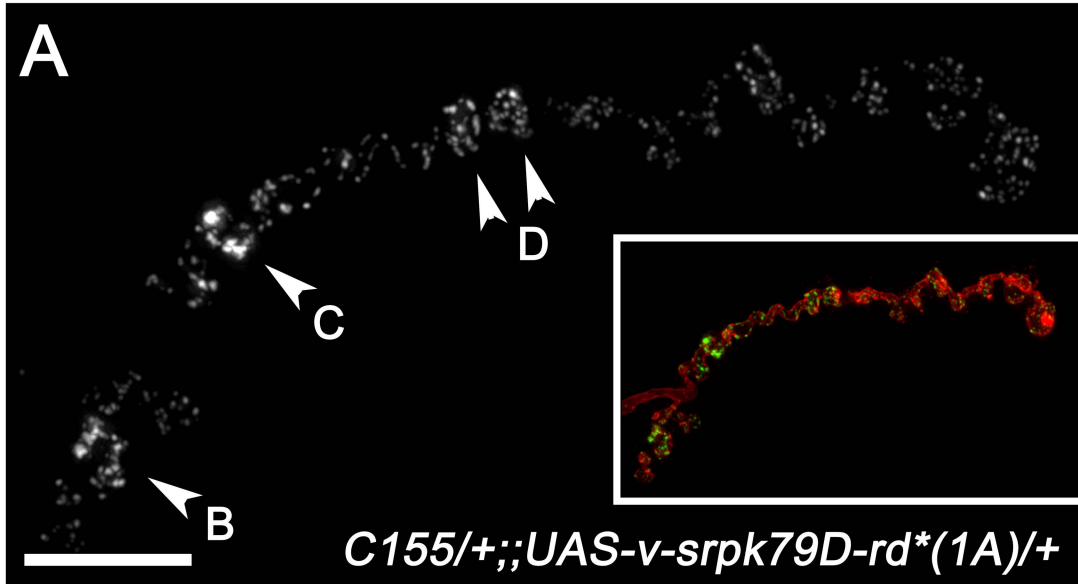
Supplemental Figure 2-4. Supplemental molecular analyses.

(A) Northern blot analysis of Brp transcripts in mRNA purified from *wild type* (left lane) or homozygous *srpk79D^{atc}* mutant (right lane) adult fly heads indicates no difference in mRNA processing between the two genotypes. Approximately 10 μ g of mRNA was loaded in each lane. An RNA sequence complementary to a region of the Brp mRNA found in all known transcripts was used to probe the blot. The lower panel shows rp49 mRNA signal as a loading control. (B) Example Western blot of protein extracted from *wild type* (left lane) or homozygous *srpk79D^{atc}* mutant (right lane) larval CNSs. There is no detectable change Brp expression levels. (B) Bar graph showing average (\pm SEM) *wild type* and *srpk79D^{atc}* anti-Brp band intensities (normalized to anti- β -Tubulin band intensity) shows that Brp is not over-expressed as a consequence of *srpk79D* loss of function. Bars represent data taken from 6 independent experiments.



Supplemental Figure 2-5. Over-expression of SRPK79D-RD* causes synaptic Brp disruption.

(A) Example anti-Brp immunofluorescence image of a muscle 4 NMJ from an animal expressing high levels of SRPK79D-RD*. Inset shows the same synapse including both anti-Brp immunofluorescence (green) and anti-HRP immunofluorescence (red) channels for orientation. Arrowheads highlight boutons with disrupted anti-Brp staining, which are magnified in (B-D). (B-D) Magnified images of highlighted boutons in (A). (E) Western blot analysis of protein extracted from three independent *UAS-v-srp79D-rd** transgenic lines showing differential protein expression. (F) Table summarizing the ability of each transgenic line in (E) to rescue the *srpk79D* mutant phenotypes and to disrupt Brp organization. Scale bar = 10 μ m.



F

	rescue	Brp disruption
28	+	-
1A	+	+
F	+	+

Supplemental Discussion Relevant to Supplemental Figure 2-8.

Two transcripts derived from the *srpk79D* locus were cloned previously as part of the Berkeley Drosophila Genome Project [Stapelton et al. 2002]. Early in our study we noticed that the cloned cDNA from the second transcript (*srpk79D-rd*) differed from the predicted splicing pattern and would lead to the production of a protein product with a truncated kinase domain. Subsequently, we used RT-PCR to confirm the existence of a transcript that conformed to the predicted splicing pattern (*srpk79D-rd**) and generated transgenic lines that express this transgene under GAL4-UAS control. This transgene rescues the Brp accumulation phenotype (Fig. 3G-3J). Thus, we are confident that *srpk79D-rd** is produced from the *srpk79D* locus and is biologically relevant.

Chapter Three:

SRPK79D is Required for Proper Homeostatic
Regulation of Synaptic Efficacy

Summary

While SRPK79D is not required for baseline synaptic function, we reasoned that this AZ-associated kinase may be important for modulating synaptic efficacy. To evaluate this hypothesis we assessed the ability of *srpk79D* mutants to perform reverse homeostatic compensation.

In *wild type*, overexpression of the vesicular glutamate transporter VGlut leads to an increase in quantal amplitude and a compensatory reduction in quantal content. We show here that VGlut overexpression in a homozygous *srpk79D* loss-of-function background causes an identical increase in quantal amplitude; however, an excessive reduction in quantal content results. That is, the degree of the reduction in quantal content is far greater than that required to compensate for the increase in quantal size. Consequently, total postsynaptic excitation is significantly diminished.

These data indicate that *srpk79D* is required for the proper execution reverse homeostasis. To our knowledge, *srpk79D* is the first gene shown to be involved in reverse homeostasis. Furthermore, as we observe excessive synaptic compensation in *srpk79D* mutants, this kinase is not required for initiation or expression of homeostatic compensation. Rather, our data suggest that SRPK79D in constrains the degree of compensation.

Introduction to Synaptic Homeostasis

Homeostatic control of cellular processes is a general theme in biology and indeed is a prerequisite for life. The fact that nervous system function persists in the face of developmental and environmental challenges, suggests that homeostatic mechanisms exist to protect neural network function as well. Current models of this “neural homeostasis” propose that deviations from baseline neural activity are detected cell-autonomously and that activity is then modulated by cell-autonomous means, for example by altering plasma membrane ratios of excitatory and inhibitory channels or by adjusting the numbers or activity synaptic neurotransmitter receptors [Turrigiano et al 1998, Marder & Prinz 2002, Davis 2006]. Alternatively, postsynaptic cells have been shown to modify their own activity by influencing the neurotransmitter release properties of their presynaptic partners [Petersen et al. 1997, DiAntonio et al. 1999, Frank et al. 2006, Branco et al. 2008, Frank et al. 2009]. Thus, non cell-autonomous forms of ‘synaptic homeostasis’ are also likely to be important for maintaining nervous system function.

The *Drosophila* neuromuscular junction has proven to be a particularly tractable system for the identification and study of genes involved in synaptic homeostasis. At this synapse perturbations that affect the average postsynaptic response to spontaneous vesicle fusion events (quantal amplitude) are compensated for by an inversely proportional modulation of the average number of synaptic vesicles that fuse in response to a presynaptic action potential (quantal content) [Petersen et al. 1997, DiAntonio et al. 1999, Frank et al. 2006, Frank et al. 2009]. Thus, the overall postsynaptic response to a presynaptic action potential (quantal amplitude x quantal content) is returned to baseline.

For example, application of the glutamate receptor antagonist philanthotoxin reduces quantal response, and in the short-term this perturbation results in a proportional decrease in the total postsynaptic response. However, a homeostatic increase in quantal content evolves over the course of approximately ten minutes and ultimately returns the total postsynaptic response to baseline [Frank et al. 2006]. We term this behavior ‘forward homeostatic compensation’. Interestingly, the *Drosophila* neuromuscular junction exhibits ‘reverse homeostatic compensation’ as well. Overexpression of the vesicular glutamate transporter (VGlut) causes an increase in the average quantal amplitude and a compensatory decrease in quantal content [Daniels et al. 2004].

Understanding of the mechanisms that underlie these homeostatic changes in vesicle release properties is of general scientific interest and may be therapeutically relevant. In particular, understanding mechanisms that downwardly modulate glutamate release (reverse homeostatic compensation) may be relevant to the prevention of excitotoxic injury that occurs in stroke and seizure.

Results

SRPK79D is required for proper execution of reverse homeostasis

Baseline synaptic function in *sprk79D* mutants is identical to *wild type* (Chapter 2, Fig 3-1A,3-1B). We reasoned however that whereas SRPK79D may be dispensable for baseline synaptic transmission, a homeostatic challenge might reveal a defect in SRPK79D-dependent signaling. Indeed we find a specific defect in reverse homeostasis in *sprk79D* mutants. VGlut overexpression in a *wild type* background leads to an increase in quantal amplitude and a compensatory decrease in quantal content [Daniels et al. 2004]. However, while an identical increase in mini amplitude is achieved by VGlut overexpression in *sprk79D* mutants, the consequent reduction in quantal content is excessive. That is, quantal content decreases to a degree that far surpasses that which would be required to compensate for the increase in quantal size (Fig 3-1A). Consequently, the average response to a presynaptic action potential is greatly diminished. In some instances the average quantal content falls to fewer than 5 quanta per action potential (Fig 3-1B).

Preliminary experiments indicate that ‘forward homeostasis’, assayed either pharmacologically (philanthotoxin) or genetically (GluRIIA mutation), is intact in *sprk79d* mutants (data not shown) [Petersen et al. 1997, DiAntonio et al. 1999, Frank et al. 2006]. Thus, SRPK79D is specifically required for the proper execution of reverse synaptic homeostasis.

Discussion

Here we show that *srpk79D* is required for the proper execution of reverse synaptic homeostasis. Specifically, increasing the quantal response by overexpressing the vesicular glutamate channel VGlut leads to a dramatic reduction in quantal content that far surpasses the appropriate compensatory response. In contrast, preliminary data suggest that forward homeostasis is intact in *srpk79D* mutants. Importantly, *srpk79D* mutation has no consequence on synaptic function in the absence of homeostatic challenge. Thus, SRPK79D plays a specific role in reverse homeostatic compensation.

These findings are novel in at least two important respects. First, *srpk79D* is the first gene shown to be involved in reverse homeostasis. Second, to our knowledge this is the first description of excessive homeostatic compensation. That is, genes implicated in synaptic homeostasis to date have been required for homeostatic initiation and/or expression. Our data indicate that homeostatic initiation is intact in *srpk79D* mutants and that *srpk79D* mutants retain the ability to express homeostatic compensation. However, the compensatory response is excessive. These data suggest that SRPK79D acts, alone or in cooperation with other proteins, as a regulator of synaptic homeostasis, providing a molecular brake on reverse homeostatic compensation.

Molecular mechanisms of reverse homeostatic compensation

Average quantal content is the product of the number of sites available for vesicle release (n) and the average probability of release at each site (P_r). It has been proposed that forward homeostatic compensation is achieved through increasing in P_r [Petersen et al. 1997, Frank et al. 2006]. The voltage-gated calcium channel $\alpha 1$ subunit Cacophony (Cac) and a signaling system involving Cac were recently shown to be required for

forward homeostasis [Frank et al. 2009]. Thus, an attractive model is that expression of forward homeostasis involves increases in Cac activity and/or number.

In contrast, very little is known about the molecular mechanisms underlying reverse homeostatic compensation. It would be interesting to know whether mutations that are required for forward homeostasis similarly affect reverse homeostasis. In light of the finding that SRPK79D is involved in reverse homeostatic compensation, Cac is an especially interesting candidate. SRPK79D regulates the assembly of the T-bar, a major constituent of which is the AZ-protein Bruchpilot (Brp). Interestingly, in *brp* mutants T-bars are absent and Cac-EGFP clustering is reduced [Kittel et al. 2006]. Thus, Brp, the T-bar and Cac may provide the molecular link between SRPK79D activity and reverse homeostatic compensation.

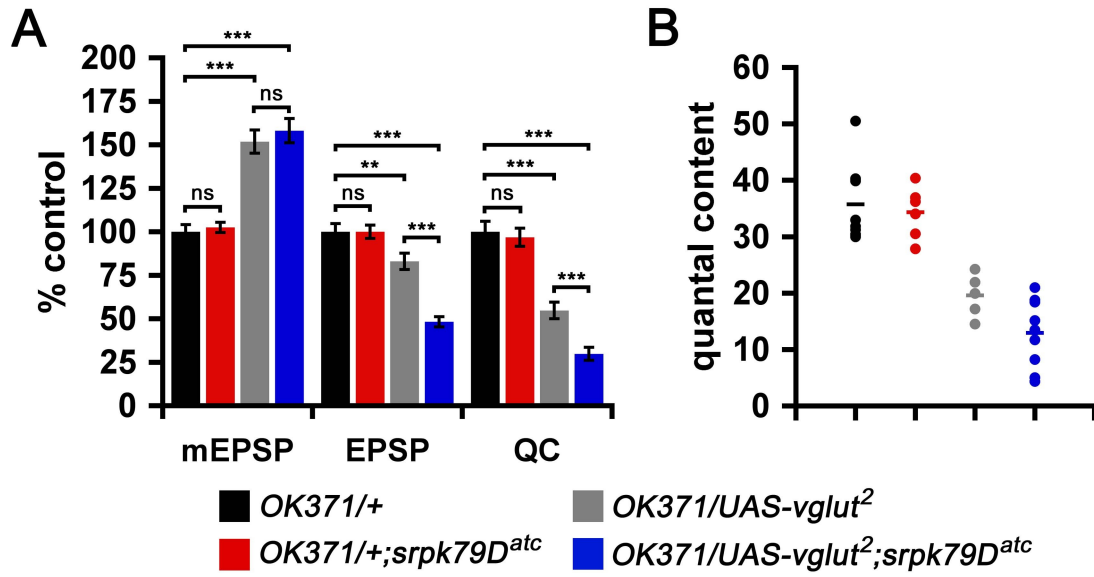
Potential models for the role of SRPK79D in homeostatic compensation

SRPK79D negatively regulates the assembly of Brp, and likely other proteins, into T-bars. Consistent with this role, SRPK79D overexpression impairs synaptic function and results in a synaptic phenotype that closely resembles that observed in *brp* mutants. These data would be consistent with a model in which SRPK79D activity could be upregulated to destabilize synaptic T-bars, thereby destabilizing synaptic Cac channels and decreasing vesicle release. This model would seem to contradict the experimental results presented in this chapter. That is, if SRPK79D were required to reduce vesicle fusion, one would predict impaired reverse homeostatic compensation in *sprk79D* loss-of-function mutants. Instead we observe excessive compensation. Thus, if we are to assume that SRPK79D's role in homeostatic compensation is related to its role in active zone assembly, a more complex model is required. Alternatively, SRPK79D may play a

direct role in promoting synaptic efficacy in the face of a reverse homeostatic challenge that is independent of its role in AZ assembly.

Figure 3-1. Improper execution of reverse homeostasis in *srpk79D* mutants

(A) Bar graphs indicating the average quantal response (mEPSP), total postsynaptic response to a presynaptic action potential (EPSP), and quantal content (QC). Mutations in *srpk79D* have no impact on baseline function. However, when provided with a reverse homeostatic challenge, quantal content is severely diminished. (B) Scatter plots showing the quantal contents of individual muscles from panel (A) (filled circles) as well as the average quantal content for each genotype (lines). ns = not significant, * = $p < 0.05$, ** = $p < 0.01$, *** = $p < 0.001$



Chapter Four:

General Conclusions

In the four decades since the active zone was first described detailed ultrastructural and molecular descriptions of its composition have emerged. In contrast, an understanding of AZ assembly mechanisms has remained elusive. Currently AZ assembly is believed to involve delivery of ‘pre-packaged’ trans-membrane and membrane-associated AZ components to nascent synapses.

This thesis describes the identification and characterization of mutants for a novel *Drosophila* serine-arginine protein kinase (SRPK79D). Loss of *srpk79D* function leads to ectopic formation of T-bar-like super-assemblies, while SRPK79D overexpression leads to disorganized synaptic AZ organization. Thus, these data extend the current understanding of AZ formation to include kinase-dependent repression of cytosolic projection assembly at non-synaptic sites and suggest that relief kinase-dependent repression underlies site-specific cytosolic projection assembly.

Interestingly, reverse homeostatic compensation is excessive in *srpk79D* mutants. To our knowledge, *srpk79D* is the first gene shown to be involved in reverse homeostatic compensation and the first gene required to prevent homeostatic overshoot. Finally, the involvement of SRPK79D in reverse homeostatic compensation suggests T-bar destabilization is involved in this process.

The conclusions made in this thesis extend the understanding of cytosolic projection assembly. However, they also suggest several more questions, several of which I address in this chapter.

Identifying the SRPK79D target

While the data in this thesis strongly implicate SRPK79D in T-bar assembly, the relevant kinase target has yet to be identified. Amino acid sequence analysis suggests that SRPK79D is a member of the serine-arginine protein kinase family, thus the target is likely an SR domain-containing protein [Nolen et al. 2001]. Genetic screens and/or biochemical approaches should be helpful in identifying this substrate.

Considerations for designing a SRPK79D target-directed genetic screen

Since the SRPK79D target is likely to be a SR protein, genes encoding this class of protein represent an ideal list of candidate genes. Fortunately, a list of SR domain-containing genes has been made available through the work of Boucher et al. who employed a bioinformatic approach to identify all SR domain-containing genes in the *Drosophila* genome [Boucher et al. 2001].

Through publically available transposon-insertion and RNAi lines, it should be possible to compile a collection of fly lines that represent putative mutants for each of these genes. However, even with this collection in hand care must be taken in designing the screen. This is because at this time it is not possible to predict whether phosphorylation tends to activate or inactivate the SRPK79D substrate, which I refer to as SR protein X (SRX). The direction of regulation has important implications for screen design.

For example, if phosphorylation tends to activate SRX, loss-of-function *srx* mutants would be expected to phenocopy the *srpk79D* mutant phenotype (normal synaptic AZs with additional T-bar-like super-assemblies). In contrast, if SRPK79D inhibits SRX, *srx* loss-of-function might be expected to impair normal T-bar assembly. This phenotype might similar to the SRPK79D overexpression phenotype (disorganized

synaptic Brp staining). However, it might also be significantly more severe. Indeed in this paradigm target loss of function might be lethal at late-embryonic or early-larval stages.

Identifying the SRPK79D target biochemically

Biochemical approaches taking advantage of the difference in phosphorylation status of SRX might also be fruitful. To this end, phospho-SR domain specific antibodies have been generated previously and used to identify differential phosphorylation status of SR proteins in sham- or SRPK2- transfected cells in culture and for immunoprecipitation [Fukuhara et al. 2006]. An effective strategy might involve Western blots of protein purified from *wild type* and *srpk79D* mutants using these antibodies to identify ‘candidate bands’ followed by immunoprecipitation and mass spectrometry.

Relieving SRPK79D-dependent assembly repression

The SRPK79D-dependent repression model implies the existence of one or more mechanisms that locally relieve repression to permit synaptic T-bar assembly the effect of which are to ‘de-phosphorylate’ SRX and/or displace it from its target. Since synaptic phosphatases have been identified and shown to play a role in development previously [Kaufmann et al. 2002, Syken et al. 2006], the possibility that relief of repression is achieved by the action of a synaptic phosphatase is especially attractive.

In this model, only SRPK79D would have access to SRX during transit from the soma to the terminal and SRX would therefore tend to be phosphorylated. Upon reaching the terminal however, the balance of kinase to phosphatase activity would be more neutral, the tendency of SRX to be de-phosphorylated would increase and T-bar assembly

would ensue. This model could be further refined to explain the site-specific assembly of T-bars, were the relevant phosphatase assumed to be localized to AZs.

A model involving a local balance between kinase and phosphatase activity is made yet more attractive by the finding that *srpk79D* is required for the proper execution of reverse homeostasis. This result suggests that local T-bar destabilization, involving *SRPK79D* and *SRX*, is an important step in this homeostatic process. Thus, consistent with other kinase-dependent forms of synaptic plasticity, dynamic control of such a process would require the presence of both a kinase and a phosphatase [Lee 2006]. Like the SR-proteins, a complete list of *Drosophila* phosphatases has been previously published [Morrison et al. 2000].

Assembly of cytosolic proteins

While the data presented in this thesis identify kinase dependent repression as a novel mechanism in the control of AZ assembly, they do not inform beyond the point of relief of repression. It is likely that determining the molecular identity of *SRX* and that of its substrates in the future will shed light on the steps involved in cytosolic projection assembly. However, to gain insight into how this process occurs in the meantime it may be informative to examine other cellular processes that involve ordered, high-density assembly of cytosolic proteins.

Centriole Assembly

Centrosomes are cellular organelles most notable for their role in mitosis. During mitotic M phase centrosomes can organize microtubules into radial arrays thereby forming the mitotic spindles that will be crucial for chromosome segregation. At the

center of the centrosome lie two organized, orthogonally oriented “barrels” called centrioles, which are surrounded by a region of peri-centriolar material (PCM). Interestingly, the PCM has been shown to form a fibrous lattice similar to the CAZ [DICTENBURG et al. 1998, NIGG 2007].

Centrioles are duplicated during S phase of each cell cycle and a considerable amount is known about the duplication process. Interestingly, in the the ‘mother’ centriole directs assembly of the ‘daughter’ centriole by concentrating the PCM, which has centriole nucleating activity [NIGG et al. 2007]. Furthermore, the balance between SAK/Plk4 kinase activity and that of an as-yet-unidentified phosphatase plays a prominent role in the regulation of ‘daughter’ centriole assembly [NIGG et al. 2007]. Unline SRPK79D however, Plk4 seems to promote rather than inhibit centriole assembly [BETTENCOURT-DIAS et al. 2005, HABEDANCK et al. 2005, NIGG 2007].

Thus, proper centriole assembly requires the localization of centriole nucleating factors in the PCM and phosphorylation-dependent regulation. T-bar assembly seems to employ a somewhat different strategy however. While T-bars are found exclusively at AZs in *wild type* larvae, in light of the finding that of T-bar-like assemblies form in *srpk79D* mutants, it is unlikely that nucleating factors are restricted to AZs. Instead, it is more likely that T-bar nucleation factors are broadly distributed in *Drosophila* motoneurons and that localized T-bar assembly involves SRPK79D-dependent restriction of nucleation activity. In this context, the SRPK79D target could be thought of as a T-bar nucleation factor that is active only in its phosphorylated state.

Ribosome Assembly

Ribosomes are molecular machines composed of both nucleotides and proteins. They are required for protein translation and as such, proper regulation of ribosome assembly is an absolute requirement for life. Ribosome assembly involves coordinated processing of ribosomal RNAs and incorporation of ribosomal protein elements. Tight control of the phosphorylation state of ribosomal proteins has also been implicated in ribosomal assembly and maturation [Staley & Woodford Jr 2009]. For example, phosphorylation and subsequent dephosphorylation of ribosomal protein S3 is required for its proper integration into the 40S ribosomal subunit [Schafer et al. 2006, Staley & Woodford Jr 2009].

While AZs have not been shown to contain nucleotides, it has recently been appreciated that the AZ ribbon structure is largely composed of two proteins that contain RNA binding domains (CtBP1 and RIBEYE/CtBP2) [Schmitz et al. 2000, tom Dieck et al. 2005]. With this in mind, it is interesting that we have identified a novel SRPK as a likely T-bar constituent since other members of this kinase family are important regulators of alternative splicing of pre-mRNAs. While we do not believe that SRPK79D is involved in mRNA processing, its presence in the T-bar suggests that some aspect of RNA handling or processing functionality may be employed/co-opted during cytosolic projection assembly.

Spliceosome Assembly

Though SRPK79D does not appear to be involved in mRNA processing, controlling alternative splicing and spliceosome composition is the best characterized role for this family of kinases. Spliceosomes are complex ‘splicing machines’ each composed of up to hundreds of protein and RNA molecules [Staley & Woodford Jr. 2009]. The

spliceosome holoenzyme is actually composed of five subcomplexes (U1, U2, U4, U5, and U6) that are incorporated in a stepwise fashion during splicing and disassembled after splicing is complete.

Given the established role for SRPKs in splicing, the importance of phosphorylation in this process is obvious. Indeed, it has long been known that cycles of phosphorylation and de-phosphorylation are required for spliceosome assembly and disassembly [Shi et al. 2006, Staley & Woodford Jr 2009]. However, the role of SRPK-mediated phosphorylation is distinct from that of other phosphorylation events. SRPK-dependent phosphorylation does not control spliceosome assembly per se, but rather regulates the subcellular SR-protein content of the spliceosome [Yeakley et al. 1999, Gravely 2000]. Other non-SRPK-dependent phosphorylation events, along with other forms of post-translational modification, in contrast are believed to control assembly of the spliceosome subcomplexes.

Thus, directly extending from the roles of SRPKs in spliceosome assembly would lead one to predict that loss of SRPK79D would change the composition of the cytosolic projection without having major impacts on cytosolic projection assembly itself. At this time, we cannot rule out the possibility that T-bar composition is altered in *srpk79D* mutants. However, given the dramatic phenotype of ectopic assembly of T-bar-like structures, SRPK79D seems to have a more general role.

Chromatin Remodeling

At first glance the connection between chromatin remodeling and T-bar assembly is not obvious. However, the formation of chromatin solves an interesting problem that may be generally relevant to cytosolic projection assembly.

Given the inherent properties of the DNA polymer, the unconstrained volume of DNA in each human cell would take up a volume approximately 5 orders of magnitude larger than the average cell nucleus [Luijsterburg et al 2008]. RNA presents a similar challenge in the cytosolic compartment. Thus, nuclear and overall cell size depends crucially on the ability to compact these molecules. The formation of chromatin and heterochromatin, are the solutions that nature has devised. That is, through three basic mechanisms (see below) DNA is compacted to the extent that it fits within a surprisingly small compartment.

Cytosolic projections are essentially the result of high-density molecular packing. Thus, while the motivation might be different, formation of cytosolic projections and other high-density structures described in this section might employ similar packing mechanisms.

DNA compaction relies on three basic strategies. The first two, supercoiling and genome folding, are likely specific to handling a long polymer and therefore less likely to be relevant to cytosolic projection assembly. The final mechanism, macromolecular crowding however, may be generally applicable to the formation of high-density protein accumulations. In short, macromolecular crowding is the entropically-driven compaction of large solutes when they are placed in a complex solution that contains small solvent particles and other small solutes [see Richter et al. 2008 and references therein for a review]. Interestingly, the concentration at which macromolecular crowding of a given large solute occurs is crucially dependent upon its molecular weight and shape. Extended, high-molecular weight solutes tend to compact at lower concentration than globular, low-molecular weight solutes [Johansson et al. 2000, Richter et al. 2008].

Thus, SRPK79D could regulate T-bar assembly by controlling the effective shape of Brp and/or other T-bar constituents by promoting interaction with another protein. For example, assume that the interaction between Brp and an SRPK79D target protein required target protein phosphorylation. Further assume that Brp tended inhabit an extended conformation when unbound, but a complex between Brp and the phosphorylated-SRPK79D target were more globular. In this paradigm unbound Brp would have a greater tendency to compact, whereas the Brp-target protein complex would be more likely to remain in solution.

Thus, constitutive phosphorylation of the SRPK79D target during Brp transport would prevent premature compaction/assembly. Upon reaching the synapse however, target protein dephosphorylation by a synaptic phosphatase for example would lead to disruption of the Brp-target protein complex. Free, extended Brp could then compact/assemble to form a T-bar. Loss of SRPK79D would also be predicted to lead to the ectopic compaction/assembly of Brp and the ectopic formation of T-bars.

This model might also explain why RNA binding proteins such as CtBP1 and RIBEYE/CtBP2 as well as proteins related to known RNA regulatory molecules such as SRPK79D appear in cytosolic projections. That is, perhaps these classes of proteins are required to facilitate macromolecular crowding and/or its regulation. A key piece of information that will speak to the validity of this and other models presented in this thesis will be the identification of SRX (the SRPK79D target). The domain structure and interaction partners of this protein will likely identify which, if any, of these models is worth pursuing.

Experimental Procedures

Fly Stocks

The listed strains were obtained from the following sources: *srpk79D[atc]* (*c00270*), *f00171*, *d09582*, *f05463*, and *d09837* from the Exelixis collection at Harvard Medical School; *v47544* (*UAS-srpk79D^{RNAi}*) from the Vienna Drosophila RNAi Collection; *P{GawB}elav^{C155}* (*C155*), *P{GawB}sca¹⁰⁹⁻⁶⁸* (*Sca*), *P{GawB}OK371* (*OK371*), *P{GAL4}repo* (*Repo*), *Khc⁸*, *Khc¹⁶*, *Df(3L)34ex5*; *dhc64C⁴⁻¹⁹*, *Df(3L)Exel6138*, *UAS-mitoGFP*, *cup¹*, *sqd^{4b4}*, *pum¹³*, *nos^{L7}*, *vas^{RJ36}*, *orb^{dec}*, *stau¹*, and *stau^{ry9}* from the Bloomington Stock Center; *Csp^{XI}* was a generous gift from Konrad Zinsmaier; *srpk79D^{VN100}* was a generous gift from Erich Buchner; *imac¹⁷⁰* was a generous gift from Thomas Schwarz; *aret^{PA}*, *aret^{PD}* and *aret^{QB}* were generous gifts from Paul MacDonald; *UAS-gfp-brp* (*UAS-g-brp*) and *brp⁶⁹* were generous gifts from Stephan Sigrist.

Immunohistochemistry

Wandering third instar larvae were dissected in calcium free saline and fixed with either 4% Paraformaldehyde/PBS (15min) or 100% Bouin's Solution (2min). Excess fixative was removed by extensive washing in PBS + 0.1% Triton-X (PBT). Dissected larvae were then incubated overnight at 4°C in PBT with one or more primary antibodies, washed in PBT, incubated either overnight (4°C) or for one hour (22°C) in PBT with one or more fluorescent-conjugated secondary antibodies, and washed again before being mounted on a slide for imaging analysis. Primary antibodies: NC82 (anti-Brp, Developmental Studies Hybridoma Bank, University of Iowa, Iowa City, IA) 1:100; 3H2 2D7 (anti-Syt, Developmental Studies Hybridoma Bank, University of Iowa, Iowa City, IA) 1:25; anti-Liprin-alpha (a generous gift from David Van Vactor) 1:1000; 1G12 (anti-DCSP-3, Developmental Studies Hybridoma Bank, University of Iowa, Iowa City, IA)

1:25; anti-Dap160 (Marie et al., 2003) 1:100. Fluorescent-conjugated secondary antibodies: goat-anti-mouse Alexa 488 (Invitrogen) 1:500; goat-anti-mouse Alexa 555 (Invitrogen) 1:500; goat-anti-rabbit Alexa 488 (Invitrogen) 1:500. Where applicable, anti-HRP-Cy3 (Jackson Immunoresearch) 1:200; anti-HRP-FITC 1:100 or anti-HRP-Cy5 1:50 were used at the same step as secondary antibody incubation. Genotypes being directly compared were grouped together during all of the above procedures.

Imaging and Analysis

Images were digitally captured using a cooled CoolSnapHQ CCD camera mounted on a Zeiss Axiovert 200M microscope. Images were acquired and analyzed using Slidebook software (Intelligent Imaging Innovations, Denver, CO). Individual nerves/synapses were optically sectioned at 0.5 μ m (11-27 sections per nerve) using a piezo-electric driven z-drive controlling the position of a Zeiss 100x oil immersion objective (NA 1.4). The intensity of anti-BRP immunostaining was quantified as follows: Each series of 0.5 μ m optical nerve sections was deconvolved (nearest-neighbors, Intelligent Imaging Innovations, Denver, CO). Two-dimensional projections of the maximum pixel intensity were then generated and the total Brp fluorescence and the maximum fluorescence intensity of each Brp punctum within the nerve/synapse area were determined for each resulting image using a semi-automated procedure as described previously [Albin & Davis 2004, Hecksher et al. 2007]. For all quantifications, the nerve/synapse area was defined as that delimited by anti-HRP staining.

Live Imaging

Live imaging was carried out as previously described [Pawson et al. 2008]. In brief, wandering third-instar larvae were dissected in HL3 saline (0.4 mM Ca^{2+}) on a

glass coverslip and held in place using pressure pins. Images were digitally captured using a Photometrics Cascade 512B camera mounted on an upright Zeiss Axioskop 2 microscope using a 100x water immersion (NA=1.0) objective and a GFP filter set (Chroma). Time lapse images were collected and analyzed using Slidebook software (Intelligent Imaging Innovations, Denver, CO).

Whole Mount mRNA *in situ* Hybridization

srpk79D mRNA was detected using a protocol based upon the “96-well plate RNA *in situ* protocol” available at the BDGP website (www.fruitfly.org). In short, mixed stage embryos were collected, fixed in 3.7% formaldehyde/1xPBS, and prepared for incubation with SP6 or T7 polymerase generated digoxigenin (DIG)-labeled nucleotide probes. To generate probes, a 954bp fragment of the *srpk79D* gene was amplified by PCR from cDNA AT02150, obtained from the Berkeley Drosophila Genome Project using primers with the sequence 5'-ttaccggattcgtccgac-3' and 5'-gcagtgattttctctccgttcgg-3'. This fragment was TA cloned into the pGEM-T Easy vector (Promega). The resulting product was used as template for T7/SP6 DIG-labeled RNA probe synthesis (Roche). After incubation and removal of excess probe, embryos were incubated with alkaline-phosphatase conjugated anti-DIG Fab fragments (Roche). Excess Fab fragments were removed by washing and a NBT/BCIP developing reaction was performed (Roche).

Northern Blots

Adult heads were removed by freezing at -70C followed by agitation. Heads were isolated using mesh filters. RNA was extracted using TRIzol reagent and standard molecular biology techniques. DIG labeled-RNA probes were generated by amplifying

an 800bp fragment of the *brp* gene from cDNA IP09541 obtained from the Berkeley Drosophila Genome Project using primers with the sequence 5'-gcaatgggcagtcactacc-3' and 5'-cccattcccttggcctgc-3' and the 738bp insert from rp49 cDNA RE59709 obtained from the Berkeley Drosophila Genome Project and 5'-cggcaaggatgtgcg-3' and 5'-actaaaagtcgggtatattaacgtttac-3' and TA cloning into pGEM-T Easy (Promega). The resulting product was used as template for T7/SP6 DIG-labeled RNA probe synthesis (Roche). Northern blot was carried out using Ambion NorthernMax-Gly protocols and reagents. Probe detection was carried out using alkaline phosphatase conjugated anti-DIG Fab fragments (Roche) in conjunction with the DIG Wash and Block Kit and CSPD Ready-to-Use.

Western Blots

Third instar larval brains were pulverized in 2x Laemmli sample buffer. Proteins were separated by SDS-PAGE and transferred to PVDF membrane. The membrane was blocked in 2% milk powder in 1xTBS-Tween, and then incubated for 1hr at room temperature with an anti-Brp monoclonal antibody (Developmental Studies Hybridoma Bank NC82, 1:100) or anti-GFP monoclonal antibody (Invitrogen 3E6, 1:100). As a protein loading control, the membrane was co-incubated with an anti- β -Tubulin monoclonal antibody (Developmental Studies Hybridoma Bank E7, 1:1000). After washing in 1xTBS-Tween, the membrane was incubated for 1hr at room temperature with horseradish peroxidase-conjugated anti-mouse secondary antibody (1:20,000), washed again and an ECL detection reaction (Amersham) was performed.

Electron Microscopy

Mutant and wild-type third-instar larvae were prepared for electron microscopy as follows. Larvae were filleted in physiological saline and fixed with 2% glutaraldehyde in 0.12 M Na-cacodylate buffer (pH 7.4, 10 min.). The fixed larvae were then transferred to vials containing fresh fixative and fixed for a total of 2 hr with rotation. Larvae were rinsed with 0.12 M Na-cacodylate buffer and postfixed with 1% osmium tetroxide in 0.12 M Na-cacodylate buffer for 1 hr. Specimens were then rinsed with 0.12 M Na-cacodylate buffer, followed by water, and then stained en bloc with 1% aqueous uranyl acetate for 1 hr. After water rinse, dehydration, and embedding in Eponate 12 resin, sections were cut with a Leica Ultracut E microtome, collected on Pioloform coated slot grids, and stained with uranyl acetate and Sato's lead. Sections were photographed with a Tecnai spirit operated at 120 kV equipped with a Gatan 4k × 4k camera.

Electrophysiology

Recordings were taken in HL3 saline (Ca^{2+} 0.4mM, Mg^{2+} 10mM) from muscle 6 in abdominal segments 2 and 3 of third-instar larvae as previously described [Davis et al. 1996]. Only recordings with resting membrane potentials more negative than -60mV and input resistances greater than $7\text{M}\Omega$ were used for analysis. Measurements of EPSP and spontaneous miniature release event amplitudes were made using MiniAnalysis software (Synapsoft, Decatur, GA).

References

Ahmari SE, Buchanan J, Smith SJ (2000) Assembly of presynaptic active zones from cytoplasmic transport packets. *Nat. Neurosci.* **3**(5):445-51.

Akins MR, Biederer T (2006) Cell-cell interactions in synaptogenesis. *Curr. Opin. Neurobiol.* **16**(1):83-9.

Albin SD, Davis GW (2004) Coordinating structural and functional synapse development: postsynaptic p21-activated kinase independently specifies glutamate receptor abundance and postsynaptic morphology. *J. Neurosci.* **24**(31):6871-9.

Anderson MJ, Cohen MW (1974) Fluorescent staining of acetylcholine receptors in vertebrate skeletal muscle. *J. Physiol.* **237**(2):385-400.

Barker DD, Wang C, Moore J, Dickinson LK, Lehmann R. (1992) Pumilio is essential for function but not for distribution of the *Drosophila* abdominal determinant Nanos **6**(12A):2312-26

Bedard KM, Daijogo S, Semler BL (2007) A nucleo-cytoplasmic SR protein functions in viral IRES-mediated translation initiation. *EMBO J.* **26**(2):459-67.

Bettencourt-Dias M, Rodrigues-Martins A, Carpenter L, Riparbelli M, Lehmann L, Gatt MK, Carmo N, Balloux F, Callaini G, Glover DM (2005) SAK/PLK4 is required for centriole duplication and flagella development. *Curr. Biol.* **15**(24):2199-207.

Blaustein M, Pelisch F, Tanos T, Muñoz MJ, Wengier D, Quadrana L, Sanford JR, Muschietti JP, Kornblihtt AR, Cáceres JF, Coso OA, Srebrow A (2005) Concerted regulation of nuclear and cytoplasmic activities of SR proteins by AKT. *Nat. Struct. Mol. Biol.* **12**(12):1037-44.

Boucher L, Ouzounis CA, Enright AJ, Blencowe BJ (2001) A genome-wide survey of RS domain proteins. *RNA* **7**(12):1693-701.

Branco T, Staras K, Darcy KJ, Goda Y. Local dendritic activity sets release probability at hippocampal synapses (2008) *Neuron* **59**(3):475-85.

Broadie KS, Bate M (1993) Development of the embryonic neuromuscular synapse of *Drosophila melanogaster*. *J. Neurosci.* **13**(1):144-66.

Buchanan J, Sun YA, Poo MM Studies of nerve-muscle interactions in *Xenopus* cell culture: fine structure of early functional contacts (1989) *J. Neurosci.* **9**(5):1540-54.

Christerson LB, McKearin DM (1994) orb is required for anteroposterior and dorsoventral patterning during *Drosophila* oogenesis *Genes Dev.* **8**(5):614-28.

Clandinin TR, Zipursky SL (2002) Making connections in the fly visual system. *Neuron*. **35**(5):827-41.

Colwill K, Feng LL, Yeakley JM, Gish GD, Cáceres JF, Pawson T, Fu XD (1996) SRPK1 and Clk/Sty protein kinases show distinct substrate specificities for serine/arginine-rich splicing factors. *J. Biol. Chem.* **271**(40):24569-75.

Connors BW, Long MA (2004) Electrical synapses in the mammalian brain. *Ann. Rev. Neurosci.* **27**:393-418.

Couteaux R, Pécot-Dechavassine M (1970) [Synaptic vesicles and pouches at the level of "active zones" of the neuromuscular junction]
C R Acad Sci Hebd Seances Acad Sci D **271**(25):2346-9.

Daniels RW, Collins CA, Gelfand MV, Dant J, Brooks ES, Krantz DE, DiAntonio A (2004) Increased expression of the *Drosophila* vesicular glutamate transporter leads to excess glutamate release and a compensatory decrease in quantal content. *J. Neurosci.* **24**(46):10466-74.

Davis GW, Schuster CM, Goodman CS (1996) Genetic dissection of structural and functional components of synaptic plasticity. III. CREB is necessary for presynaptic functional plasticity. *Neuron* **17**(4):669-79.

Davis GW, Schuster CM, Goodman CS (1997) Genetic analysis of the mechanisms controlling target selection: target-derived Fasciclin II regulates the pattern of synapse formation. *Neuron* **19**(3):561-73.

Davis GW (2006) Homeostatic control of neural activity: from phenomenology to molecular design. *Annu. Rev. Neurosci.* **29**:307-23.

DiAntonio A, Petersen SA, Heckmann M, Goodman CS (1999) Glutamate receptor expression regulates quantal size and quantal content at the *Drosophila* neuromuscular junction. *J. Neurosci.* **19**(8):3023-32.

Dicthenberg JB, Zimmerman W, Sparks CA, Young A, Vidair C, Zheng Y, Carrington W, Fay FS, Doxsey SJ (1998) Pericentrin and gamma-tubulin form a protein complex and are organized into a novel lattice at the centrosome. *J. Cell Biol.* **141**(1):163-74.

Dick O, tom Dieck S, Altrock WD, Ammermuller J, Weiler R, Garner CC, Gundelfinger ED, Brandstatter JH (2003) The presynaptic active zone protein bassoon is essential for photoreceptor ribbon synapse formation in the retina. **37**(5):775-86.

Dresbach T, Torres V, Wittenmayer N, Altrock WD, Zamorano P, Zuschratter W, Nawrotzki R, Ziv NE, Garner CC, Gundelfinger ED (2006) Assembly of active zone

precursor vesicles: obligatory trafficking of presynaptic cytomatrix proteins Bassoon and Piccolo via a trans-Golgi compartment. *J Biol Chem.* **281**(9):6038-47.

Eberle KK, Zinsmaier KE, Buchner S, Gruhn M, Jenni M, Arnold C, Leibold C, Reisch D, Walter N, Hafen E, Hofbauer A, Pflugfelder GO, Buchner E (1998) Wide distribution of the cysteine string proteins in *Drosophila* tissues revealed by targeted mutagenesis. *Cell Tissue Res.* **294**(2):203-17.

Eldon ED, Pirrotta V (1991). Interactions of the *Drosophila* gap gene giant with maternal and zygotic pattern-forming genes. *Development* **111**(2):367-78.

Fernandez-Chacon R, Wölfel M, Nishimune H, Tabares L, Schmitz F, Castellano-Muñoz M, Rosenmund C, Montesinos ML, Sanes JR, Schneggenburger R, Sudhof TC (2004) The synaptic vesicle protein CSP alpha prevents presynaptic degeneration. *Neuron* **42**(2):237-51.

Frank CA, Kennedy MJ, Goold CP, Marek KW, Davis GW (2006) Mechanisms underlying the rapid induction and sustained expression of synaptic homeostasis. *Neuron* **52**(4):663-77.

Frank CA, Pielage J, Davis GW (2009) A presynaptic homeostatic signaling system composed of the Eph receptor, ephexin, Cdc42, and CaV2.1 calcium channels. *Neuron* **61**(4):556-69.

Fukuhara T, Hosoya T, Shimizu S, Sumi K, Oshiro T, Yoshinaka Y, Suzuki M, Yamamoto N, Herzenberg LA, Herzenberg LA, Hagiwara M (2006) Utilization of host SR protein kinases and RNA-splicing machinery during viral replication. *Proc Natl Acad Sci U S A.* **103**(30):11329-33.

Gepner J, Li M, Ludmann S, Kortas C, Boylan K, Iyadurai SJ, McGrail M, Hays TS (1996) Cytoplasmic dynein function is essential in *Drosophila melanogaster*. *Genetics* **142**(3):865-78.

Gindhart JG Jr, Desai CJ, Beushausen S, Zinn K, Goldstein LS (1998) Kinesin light chains are essential for axonal transport in *Drosophila*. *J. Cell Biol.* **141**(2):443-54.

Goda Y, Davis GW (2003) Mechanisms of synapse assembly and disassembly. *Neuron* **40**(2):243-64.

Graveley BR (2000) Sorting out the complexity of SR protein functions. *RNA* **6**(9):1197-211.

Guo X, Macleod GT, Wellington A, Hu F, Panchumarthi S, Schoenfield M, Marin L, Charlton MP, Atwood HL, Zinsmaier KE (2005) The GTPase dMiro is required for axonal transport of mitochondria to *Drosophila* synapses. *Neuron* **47**(3):379-93.

- Habedanck R, Stierhof YD, Wilkinson CJ, Nigg EA (2005) The Polo kinase Plk4 functions in centriole duplication. *Nat. Cell Biol.* **7**(11):1140-6.
- Harlow ML, Ress D, Stoschek A, Marshall RM, McMahan UJ (2001) The architecture of active zone material at the frog's neuromuscular junction. *Nature.* **409**(6819):479-84.
- Heckscher ES, Fetter RD, Marek KW, Albin SD, Davis GW (2007) NF-kappaB, IkappaB, and IRAK control glutamate receptor density at the Drosophila NMJ. *Neuron* **55**(6):859-73.
- Huang Y, Steitz JA (2005) SRprises along a messenger's journey. *Mol. Cell* **17**(5):613-5.
- Hurd DD, Saxton WM. Kinesin mutations cause motor neuron disease phenotypes by disrupting fast axonal transport in Drosophila (1996) *Genetics* **144**(3):1075-85.
- Jack TP, McGinnis W (1990) Establishment of the Deformed expression stripe requires the combinatorial action of coordinate, gap and pair-rule proteins. *EMBO J.* **9**(4):1187-98.
- Johansson HO, Brooks DE, Haynes CA (2000) Macromolecular crowding and its consequences. *Int. Rev. Cytol.* **192**:155-70.
- Jontes JD, Buchanan J, Smith SJ (2000) Growth cone and dendrite dynamics in zebrafish embryos: early events in synaptogenesis imaged in vivo. *Nat. Neurosci.* **3**(3):231-7.
- Kaesler PS, Sudhof TC (2005) RIM function in short- and long-term synaptic plasticity. *Biochem. Soc. Trans.* **33**(Pt 6):1345-9.
- Kaufmann N, DeProto J, Ranjan R, Wan H, Van Vactor D (2002) Drosophila liprin-alpha and the receptor phosphatase Dlar control synapse morphogenesis. *Neuron* **34**(1):27-38.
- Kawasaki F, Zou B, Xu X, Ordway RW (2004) Active zone localization of presynaptic calcium channels encoded by the cacophony locus of Drosophila. *J. Neurosci.* **24**(1):282-5
- Keyes LN, Spradling AC (1997) The Drosophila gene fs(2)cup interacts with out to define a cytoplasmic pathway required for the structure and function of germ-line chromosomes **124**(7):1419-31.
- Khimich D, Nouvian R, Pujol R, Tom Dieck S, Egner A, Gundelfinger ED, Moser T (2005) Hair cell synaptic ribbons are essential for synchronous auditory signalling. *Nature.* **434**(7035):889-94.

- Kindler S, Wang H, Richter D, Tiedge H (2005) RNA transport and local control of translation. *Annu. Rev. Cell Dev. Biol.* **21**:223-45.
- Kittel RJ, Wichmann C, Rasse TM, Fouquet W, Schmidt M, Schmid A, Wagh DA, Pawlu C, Kellner RR, Willig KI, Hell SW, Buchner E, Heckmann M, Sigris SJ (2006) Bruchpilot promotes active zone assembly, Ca²⁺ channel clustering, and vesicle release. *Science* **312**(5776):1051-4.
- Koizumi J, Okamoto Y, Onogi H, Mayeda A, Krainer AR, Hagiwara M (1999) The subcellular localization of SF2/ASF is regulated by direct interaction with SR protein kinases (SRPKs). *J. Biol. Chem.* **274**(16):11125-31.
- Kraut R, Levine M (1991) Spatial regulation of the gap gene giant during Drosophila development. *Development* **111**(2):601-9.
- Lantz V, Chang JS, Horabin JI, Bopp D, Schedl P (1994) The Drosophila orb RNA-binding protein is required for the formation of the egg chamber and establishment of polarity. *Genes Dev.* **8**(5):598-613.
- Lee (2006) Synaptic plasticity and phosphorylation. *Pharmacol. Ther.* **112**(3):810-32
- Leung KM, van Horck FP, Lin AC, Allison R, Standart N, Holt CE (2006) Asymmetrical beta-actin mRNA translation in growth cones mediates attractive turning to netrin-1. *Nat. Neurosci.* **9**(10):1247-56.
- Magupalli VG, Schwarz K, Alpaadi K, Natarajan S, Seigel GM, Schmitz F (2008) Multiple RIBEYE-RIBEYE interactions create a dynamic scaffold for the formation of synaptic ribbons. *J Neurosci.* **28**(32):7954-67.
- Marder E, Prinz AA (2002) Modeling stability in neuron and network function: the role of activity in homeostasis. *Bioessays.* **24**(12):1145-54.
- Martin M, Iyadurai SJ, Gassman A, Gindhart JG Jr, Hays TS, Saxton WM (1999) Cytoplasmic dynein, the dynactin complex, and kinesin are interdependent and essential for fast axonal transport. *Mol. Biol. Cell* **10**(11):3717-28.
- McCabe BD, Marqués G, Haghghi AP, Fetter RD, Crotty ML, Haerry TE, Goodman CS, O'Connor MB (2003) The BMP homolog Gbb provides a retrograde signal that regulates synaptic growth at the Drosophila neuromuscular junction. *Neuron* **39**(2):241-54.
- Miller KE, DeProto J, Kaufmann N, Patel BN, Duckworth A, Van Vactor D (2005) Direct observation demonstrates that Liprin-alpha is required for trafficking of synaptic vesicles. *Curr. Biol.* **15**(7):684-9.

- Miron M, Lasko P, Sonenberg N (2003) Signaling from Akt to FRAP/TOR targets both 4E-BP and S6K in *Drosophila melanogaster*. *Mol. Cell Biol.* **23**(24):9117-26.
- Morrison DK, Murakami MS, Cleghon V (2000) Protein kinases and phosphatases in the *Drosophila* genome. *J. Cell Biol.* **150**(2):F57-62
- Nieratschker V, Bloch A, Bock N, Bucher D, Dippacher S, Jauch M, Krohne G, Asan E, Buchner S, and Buchner E (in review) Bruchpilot aggregates, behavioral defects, and early death in SRPK79D kinase mutants of *Drosophila*. *Plos Genetics*
- Nigg EA (2007) Centrosome duplication: of rules and licenses. *Trends Cell Biol.* **17**(5):215-21
- Nolen B, Yun CY, Wong CF, McCammon JA, Fu XD, Ghosh G (2001) The structure of Sky1p reveals a novel mechanism for constitutive activity. *Nat. Struct. Biol.* **8**(2):176-83.
- Pack-Chung E, Kurshan PT, Dickman DK, Schwarz TL (2007) A *Drosophila* kinesin required for synaptic bouton formation and synaptic vesicle transport. *Nat. Neurosci.* **10**(8):980-9.
- Pawson C, Eaton BA, Davis GW (2008) Formin-dependent synaptic growth: evidence that Dlar signals via Diaphanous to modulate synaptic actin and dynamic pioneer microtubules. *J. Neurosci.* **28**(44):11111-23
- Petersen SA, Fetter RD, Noordermeer JN, Goodman CS, DiAntonio A (1997) Genetic analysis of glutamate receptors in *Drosophila* reveals a retrograde signal regulating presynaptic transmitter release. *Neuron* **19**(6):1237-48.
- Pilling AD, Horiuchi D, Lively CM, Saxton WM (2006) Kinesin-1 and Dynein are the primary motors for fast transport of mitochondria in *Drosophila* motor axons. *Mol. Biol. Cell* **17**(4):2057-68.
- Richter K, Nessling M, Lichter P (2008) Macromolecular crowding and its potential impact on nuclear function. *Biochim. Biophys. Acta.* **1783**(11):2100-7.
- Rizo J, Rosenmund C (2008) Synaptic vesicle fusion. *Nat. Struct. Mol. Biol.* **15**(7):665-74.
- Sanes JR, Lichtman JW (1999) Development of the vertebrate neuromuscular junction. *Annu. Rev. Neurosci.* **22**:389-442.
- Schafer T, Maco B, Petfalski E, Tollervey D, Böttcher B, Aebi U, Hurt E (2006) Hrr25-dependent phosphorylation state regulates organization of the pre-40S subunit. *Nature* **441**(7093):651-5.

- Shi Y, Reddy B, Manley JL (2006) PP1/PP2A phosphatases are required for the second step of Pre-mRNA splicing and target specific snRNP proteins. *Mol. Cell* **23**(6):819-29.
- Schmitz F, Konigstorfer A, Sudhof TC (2000) RIBEYE, a component of synaptic ribbons: a protein's journey through evolution provides insight into synaptic ribbon function. *Neuron* **28**(3):857-72.
- Schoch S, Gundelfinger ED (2006) Molecular organization of the presynaptic active zone. *Cell Tissue Res.* **326**(2):379-91.
- Schuster CM, Davis GW, Fetter RD, Goodman CS (1996) Genetic dissection of structural and functional components of synaptic plasticity. I. Fasciclin II controls synaptic stabilization and growth. *Neuron* **17**(4):641-54.
- Shapira M, Zhai RG, Dresbach T, Bresler T, Torres VI, Gundelfinger ED, Ziv NE, Garner CC (2003) Unitary assembly of presynaptic active zones from Piccolo-Bassoon transport vesicles. *Neuron* **38**(2):237-52.
- Shen K, Fetter RD, Bargmann CI (2004) Synaptic specificity is generated by the synaptic guidepost protein SYG-2 and its receptor, SYG-1. *Cell* **116**(6):869-81.
- Staley JP, Woolford JL Jr (2009) Assembly of ribosomes and spliceosomes: complex ribonucleoprotein machines. *Curr. Opin. Cell Biol.* **21**(1):109-18.
- Steinhauer J, Kalderon D (2005) The RNA-binding protein Squid is required for the establishment of anteroposterior polarity in the *Drosophila* oocyte. *Development* **132**(24):5515-25.
- Stapleton M, Brokstein P, Hong L, Agbayani A, Carlson J, Champe M, Chavez C, Dorsett V, Dresnek D, Farfan D, Frise E, George R, Gonzalez M, Guarin H, Kronmiller B, Li P, Liao G, Miranda A, Mungall CJ, Nunoo J, Pacleb J, Paragas V, Park S, Patel S, Phouanavong S, Wan K, Yu C, Lewis SE, Rubin GM, Celniker S (2002) Direct submission. Berkeley *Drosophila* Genome Project, Lawrence Berkeley National Laboratory.
- Sutton MA, Schuman EM (2006) Dendritic protein synthesis, synaptic plasticity, and memory. *Cell* **127**(1):49-58.
- Syken J, Grandpre T, Kanold PO, Shatz CJ (2006) PirB restricts ocular-dominance plasticity in visual cortex. *Science* **313**(5794):1795-800.
- Thibault ST, Singer MA, Miyazaki WY, Milash B, Dompe NA, Singh CM, Buchholz R, Demsky M, Fawcett R, Francis-Lang HL, Ryner L, Cheung LM, Chong A, Erickson C, Fisher WW, Greer K, Hartouni SR, Howie E, Jakkula L, Joo D, Killpack K, Laufer A, Mazzotta J, Smith RD, Stevens LM, Stuber C, Tan LR, Ventura R, Woo A, Zakrajsek I,

Zhao L, Chen F, Swimmer C, Kopczyński C, Duyk G, Winberg ML, Margolis J (2004) A complementary transposon tool kit for *Drosophila melanogaster* using P and piggyBac. *Nat. Genet.* **36**(3):283-7.

Tinker R, Silver D, Montell DJ (1998) Requirement for the vasa RNA helicase in gurken mRNA localization *Dev. Biol.* **199**(1):1-10

tom Dieck S, Altrock WD, Kessels MM, Qualmann B, Regus H, Brauner D, Fejtová A, Bracko O, Gundelfinger ED, Brandstätter JH (2005) Molecular dissection of the photoreceptor ribbon synapse: physical interaction of Bassoon and RIBEYE is essential for the assembly of the ribbon complex. *J. Cell Biol.* **168**(5):825-36.

Turrigiano GG, Leslie KR, Desai NS, Rutherford LC, Nelson SB (1998) Activity-dependent scaling of quantal amplitude in neocortical neurons. *Nature.* **391**(6670):892-6.

Varoqueaux F, Sigler A, Rhee JS, Brose N, Enk C, Reim K, Rosenmund C (2002) Total arrest of spontaneous and evoked synaptic transmission but normal synaptogenesis in the absence of Munc13-mediated vesicle priming. *Proc. Natl. Acad. Sci. USA.* **99**(13):9037-42.

Wagh DA, Rasse TM, Asan E, Hofbauer A, Schwenkert I, Dürrbeck H, Buchner S, Dabauvalle MC, Schmidt M, Qin G, Wichmann C, Kittel R, Sigrist SJ, Buchner E (2006) Bruchpilot, a protein with homology to ELKS/CAST, is required for structural integrity and function of synaptic active zones in *Drosophila*. *Neuron* **49**(6):833-44.

Zhai RG & Bellen HJ (2004) The architecture of the active zone in the presynaptic nerve terminal. *Physiology (Bethesda)* **19**:262-70.

Webster PJ, Liang L, Berg CA, Lasko P, Macdonald PM (1997) Translational repressor bruno plays multiple roles in development and is widely conserved. *Genes Dev.* **11**(19):2510-21.

Wu KY, Hengst U, Cox LJ, Macosko EZ, Jeromin A, Urquhart ER, Jaffrey SR (2005) Local translation of RhoA regulates growth cone collapse. *Nature* **436**(7053):1020-4.

Ye B, Zhang Y, Song W, Younger SH, Jan LY, Jan YN (2007) Growing dendrites and axons differ in their reliance on the secretory pathway. *Cell* **130**(4):717-29.

Yeakley JM, Tronchère H, Olesen J, Dyck JA, Wang HY, Fu XD (1999) Phosphorylation regulates in vivo interaction and molecular targeting of serine/arginine-rich pre-mRNA splicing factors. *J. Cell. Biol.* **145**(3):447-55.

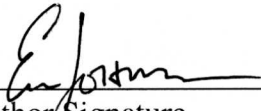
Zhai RG, Vardinon-Friedman H, Cases-Langhoff C, Becker B, Gundelfinger ED, Ziv NE, Garner CC (2001) Assembling the presynaptic active zone: a characterization of an active one precursor vesicle. *Neuron* **29**(1):131-43.

Publishing Agreement

It is the policy of the University to encourage the distribution of all theses, dissertations, and manuscripts. Copies of all UCSF theses, dissertations, and manuscripts will be routed to the library via the Graduate Division. The library will make all theses, dissertations, and manuscripts accessible to the public and will preserve these to the best of their abilities, in perpetuity.

Please sign the following statement:

I hereby grant permission to the Graduate Division of the University of California, San Francisco to release copies of my thesis, dissertation, or manuscript to the Campus Library to provide access and preservation, in whole or in part, in perpetuity.



Author Signature

5/26/09
Date